# Hydrogen-natural gas combustion in a marine lean-burn SI engine
## A comparitive analysis of Seiliger and double Wiebe function-based zero–dimensional modelling

Sapra, Harsh; Godjevac, Milinko; De Vos, Peter; Van Sluijs, Wim; Linden, Youri; Visser, Klaas

**Citation (APA)**
Sapra, H., Godjevac, M., De Vos, P., Van Sluijs, W., Linden, Y., & Visser, K. (2020). Hydrogen-natural gas combustion in a marine lean-burn SI engine: A comparitive analysis of Seiliger and double Wiebe function-based zero–dimensional modelling. *Energy Conversion and Management*, *207*, Article 112494. https://doi.org/10.1016/j.enconman.2020.112494

**Important note**
To cite this publication, please use the final published version (if applicable).
Please check the document version above.

# HYDROGEN-NATURAL GAS COMBUSTION IN A MARINE LEAN-BURN SI ENGINE: A COMPARATIVE ANALYSIS OF SEILIGER AND DOUBLE WIEBE FUNCTION-BASED ZERO–DIMENSIONAL MODELLING

**Harsh Sapra[a*], Milinko Godjevac[b], Peter De Vos[a], Wim Van Sluijs[c], Youri Linden[d], Klaas Visser[a]**

*Corresponding author email-id: h.d.sapra@tudelft.nl
[a] Faculty of Mechanical, Maritime and Materials Engineering, Delft University of Technology, The Netherlands
[b] Allseas Engineering B.V., Delft, The Netherlands
[c] Pon Power Nederland, Papendrecht, The Netherlands
[d] Defence Material Organization, Ministry of Defence, Utrecht, The Netherlands

## ABSTRACT

With increasingly stringent emission regulations, marine natural gas engines need to improve their performance. Various proven advantages of hydrogen-natural gas (H-NG) blends make them a promising enhanced fuel solution. Although modelling of H-NG combustion has been investigated before, mostly using CFD models, the literature on the modelling capabilities of Seiliger-based and Wiebe-based zero-dimensional (0-D) models is limited for H-NG combustion. Especially for the application of marine lean-burn spark-ignited (SI) engines. Therefore, the aim of this paper is to compare the capabilities of Seiliger-based and double Wiebe function-based 0-D models to capture H-NG combustion in a marine SI engine for different H-NG fuel blends, engine leaning (lean-burn operation) and engine loads.

In this work, measurements on a turbocharged, SI marine natural gas engine were used to develop a heat release rate model, which was subsequently used as a basis for the Seiliger and double Wiebe function-based H-NG combustion characterization models. Results from the two combustion modelling approaches were compared for different H-NG fuel blends, engine leaning (lean-burn operation) and engine loads. The modelling results were also compared against engine measurements for different experimental conditions.

This paper shows that the Seiliger modelling approach can be used to define different physical phenomenon in H-NG combustion, while accurately capturing the effects of hydrogen addition and engine leaning on the H-NG combustion process at varying engine loads. This research also found that the variations in late burn phase present in lean-burn NG and H-NG combustion can be captured using the double-Wiebe modelling approach, however, clear trends of the Wiebe combustion parameters for varying fuel blends and engine loads could not be identified to accurately capture the H-NG combustion process. Furthermore, Wiebe-based modelling approach produced larger errors in the estimations of work output and combustion heat for all test conditions.

## KEYWORDS

Hydrogen-Natural gas; Marine SI engine; Seiliger model; Wiebe model; Lean-burn combustion

## NOMENCLATURE

| | | | |
|---|---|---|---|
| $p$ | Pressure (bar) | **Acronyms** | |
| $T$ | Temperature (K) | ICE | Internal combustion engine |
| $V$ | Volume ($m^3$) | TDC | Top Dead Center |
| $M$ | Mass (kg) | BDC | Bottom Dead Center |
| $T$ | Time (seconds) or Trapped | SI | Spark-ignited |
| $c_v$ | Specific heat at constant volume (kJ/kgK) | MVEM | Mean value engine model |
| $c_p$ | Specific heat at constant pressure (kJ/kgK) | 0-D | Zero-dimensional |
| $ϒ$ | Ratio specific heats | RCO | Reaction Co-ordinate |
| $λ$ | Air-excess ratio | CRR | Combustion Reaction Rate |
| $t$ | Trapped | HRR | Heat Release Rate |
| $R$ | Gas Constant (kJ/kgK) | Max | Maximum |
| $Q$ | Heat (kJ) | NOx | Nitrogen oxides (mg/$Nm^3$) or (g/kWh) |
| $q$ | Specific heat quantity (kJ/kg) | $O_2$ | Oxygen |
| CA | Crank angle (degree) | H | Hydrogen |
| $u_{comb-fuel}$ | Effective heat of combustion (kJ/kg) | NG | Natural gas |
| $W$ | Work (kJ) | Norm | Normalized |
| $w$ | Specific work quantity (kJ/kg) | SOC | Start of combustion |
| 'a' | Seiliger parameter 'a' | EOC | End Of Combustion |
| 'b' | Seiliger parameter 'b' | 0H-NG | 0% Hydrogen and 100% Natural gas blend |
| 'c' | Seiliger parameter 'c' | 5H-NG | 5% Hydrogen and 95% Natural gas blend |
| $r_c$ | Effective compression ratio | 10H-NG | 10% Hydrogen and 90% Natural gas blend |
| $r_e$ | Effective expansion ratio | 20H-NG | 20% Hydrogen and 80% Natural gas blend |
| $n_c$ | Polytropic compression coefficient | | |
| $n_e$ | Polytropic expansion coefficient | **Units** | |
| $η_c$ | Polytropic compression factor | Bar | Bar |
| $η_c$ | Polytropic expansion factor | kW | Kilowatt |
| $m_1, m_2$ | Wiebe shape parameters | rpm | Revolutions per minute |
| $b_1, b_2$ | Wiebe combustion weighing factors | K | Kelvin |
| $a_1, a_2$ | Wiebe combustion efficiency factors | kg | Kilogram |
| $η_c$ | Combustion efficiency | mg | Milligram |
| $CD_1$ | Combustion duration for $1^{st}$ Wiebe | $Nm^3$ | Normal cubic meter |
| $CD_2$ | Combustion duration for $2^{nd}$ Wiebe | kJ | Kilojoule |
| $H_v$ | Volumetric hydrogen percentage | m | Meter |
| $i$ | Number of cylinders | $^0$ or deg | Degree |
| $k$ | Number of revolution per cycle | g/kWh | gram per kilowatt-hour |
| $ρ$ | Density (kg/$m^3$) | % | Percentage |
| cg | Combustion gas | | |
| rg | Residual gas | | |
| f | Fuel | | |
| x | Mass fraction | | |
| σ | Stoichiometric air-to-fuel ratio | | |

# 1   INTRODUCTION

In recent years, lean-burn natural gas (NG) engines have gained interest for maritime applications due to various attractive qualities such as high thermal efficiencies, low NOx emissions, reduced risk of knocking and the possibility of high-compression ratios [1]–[3]. However, low flame propagation speed and high ignition temperature of natural gas deteriorate its combustion and restrict the engine operation between the knock and misfire limits. For maritime applications, the restricted operating window reduces further as marine spark-ignited (SI) engines operate at high brake mean effective pressures [4]–[6]. The limited operating window also restricts the load-taking capabilities of these marine engines and retards their application to generator mode and electric ship propulsion, which results in lower overall efficiency due to conversion losses [7]–[9]. However, researchers have shown that blending hydrogen with natural gas can enhance the lean-burn capabilities of natural gas engines due to the high laminar flame speed of hydrogen, which can extend the operating window [8], [10]. Hydrogen blending also helps in reducing carbon dioxide and carbon monoxide emissions of natural gas engines [8]. Various proven advantages of hydrogen-natural gas (H-NG) blends such as increased flammability limits, high flame speed, hydrogen renewability, high volumetric calorific value and reduced unburnt hydrocarbon emissions make hydrogen-natural gas a promising fuel for marine engines.

The development of engine technology is extensively supported by model simulations. Models can help improve engine design, understanding of in-cylinder chemical and physical processes, their overall performance and transient capabilities [11]–[14]. The choice of engine modelling approach can vary from detailed computational fluid dynamics (CFD) models to straight forward transfer function models depending on the required accuracy, amount of information and computational time required. The specific choice of CFD models helps to acquire detailed process information with a high degree of model complexity and computational time [15]–[17]. Numerous CFD studies have been performed to study engine performance with diesel as well as alternative fuels such as H-NG, methanol and DME [18]–[21]. Followed by CFD models, in terms of complexity, are one-dimensional and quasi-dimensional thermodynamic models [22], [23]. In addition to multiple dimensions, the combustion process can be studied as single-zone, two-zone and multi-zone combustion models. In single-zone models, the working fluid undergoing the combustion process is assumed to be lumped into a single thermodynamic control volume [24], [25]. On the other hand, the working fluid is split between a burned and an unburned thermodynamic control volume (or zone) in a two-zone model and several zones in a multi-zone model [26]. Although multi-dimensional models provide detailed predictions of the combustion process, zero-dimensional (0-D) thermodynamic models are often applied due to their ability to capture the in-cylinder combustion process with reduced computational effort as they are relatively simpler [27], [28]. 0-D combustion models are practical as they provide quick and helpful results to study engine performance, however, the simulation results can have reduced accuracy and details.

A 0-D model by definition has no spatial resolution and does not provide any information on the dynamics of fluid within the process. A commonly adopted approach for 0-D combustion models is to employ the empirical Wiebe model to simulate the fuel mass-burn rate and compute the combustion energy released. The combustion process can be represented by single or multiple Wiebe functions, which are mathematically defined by single or multiple Wiebe coefficients for combustion efficiency, shape factor and combustion duration [29], [30]. In SI natural gas engines, the combustion is divided into three phases of flame development, propagation and termination, which have different combustion rates [31]. For instance. The flame termination phase is very slow as compared to the other two phases. A single Wiebe function with three coefficients can struggle in precisely capturing all the three combustion phases with different alternative fuels, fuel blends, injection strategies and lean operating conditions. Based on this understanding, Yildiz et. al. [27] compared the capabilities of single and double Wiebe functions to reproduce the experimental in-cylinder pressures and gross indicated mean effective pressure (GIMEP) for methane and hydrogen-methane blends in a 500 cc SI engine. They concluded that double Wiebe functions fitted better than the single-Wiebe functions, however, discussions on the capabilities of double Wiebe function to simulate in-cylinder temperatures, combustion heat and work at varying engine loads and lean operating conditions were not provided. Furthermore, Liu et. al. [32] showed that the standard single Wiebe function was unable to predict the mass-burn fraction in a single-cylinder diesel engine converted to a natural gas SI engine. However, a modified double Wiebe function for the slower burning process inside the squish region performed better. They also concluded that such a condition-dependent double Wiebe model is limited to the operating conditions used for determining the model parameters. Furthermore, most of the studies employing Wiebe modelling for gaseous fuel combustion are focussed on automotive or small scale engines [33]–[35]. In NG engines, the stability of the combustion process affects the operating window between knock and misfire limits [8]. The operating window

of marine NG engines reduces as the brake mean effective pressure (BMEP) scales upwards [5], [6]. Marine engines also operate at lower engine speeds, thus, increasing the combustion process time. Additionally, marine engines have less heat loss due to the larger combustion chamber volume to surface area ratio compared to automotive engines. The lower heat loss in marine engines has a direct impact on the combustion heat, work in-cylinder pressures and temperatures. Therefore, the performance and combustion within a marine SI NG engine can vary from that of an automobile engine. However, it is unclear if the scaling effects in marine SI engines for lean H-NG combustion are captured using Wiebe modelling.

Other than Wiebe functions, another approach that could be adopted for 0-D combustion models is the Seiliger process modelling approach. Like Wiebe in 0-D combustion models, a Seiliger process model also does not provide any spatial or fluid dynamic related information. Seiliger cycle is a variation of the thermodynamic dual cycle used to define the in-cylinder processes [36], [37]. The Seiliger process uses finite, discretised stages to describe the in-cylinder process out of which three stages divided into isochoric, isobaric and isothermal processes are used to capture the combustion process [37]. Therefore, Seiliger is a first-principle, thermodynamic approach to capture the in-cylinder and combustion process compared to the semi-empirical Wiebe functions [29]. Moreover, Wiebe provides an estimation of the combustion and in-cylinder process per crank angle, while Seiliger discretises the same process into finite stages and estimates in-cylinder information at all the critical points using the Seiliger combustion parameters [37]. Therefore, Seiliger cannot provide information pertaining to crank-angle events such as CA10, CA50, CA90 and maximum rate of pressure rise, unlike the Wiebe modelling approach. However, the Seiliger modelling approach provides sufficient details of the in-cylinder and combustion process that can be captured with low computational effort. This makes the Seiliger modelling approach in combination with Mean Value Engine Models (MVEMS) ideal for studying load variations, system integration, control strategies, voyage simulations and smart maintenance of ships. Sui et.al. fitted the Seiliger cycle for diesel combustion in a MVEM [38], [39]. Similarly, Georgescu et. al. adopted the Seiliger cycle for a dual-fuel natural gas engine to study the dynamic behaviour based on MVEM simulations [40], [41]. Skogtjarn [42] used the Seiliger cycle for estimation of exhaust gas temperatures in diesel engines. Appendix 1 lists all the parameters that can be estimated using the Wiebe and Seiliger modelling approach.

In the current literature, Seiliger process modelling has been mainly limited to capturing diesel combustion as part of system-level investigations. There is a lack of comprehensive investigations on the capabilities of Seiliger process modelling in capturing combustion of gaseous fuels such as H-NG fuel blends. Furthermore, the above literature survey of Wiebe-based modelling highlights that the Wiebe function coefficients and their capabilities to capture combustion vary with operating conditions, combustion modes, type of fuel and fuel blends. It also indicates limited literature on a comprehensive analysis of the capabilities of a double Wiebe function in capturing lean-burn combustion of hydrogen-natural gas blends in a marine SI engine. Additionally, there is no literature that compares the capabilities of these two modelling approaches in capturing the H-NG combustion process. Therefore, the goal of this paper is to compare the capabilities of the first-principle Seiliger-based and semi-empirical double Wiebe function-based modelling approaches in capturing H-NG combustion. The model results are studied and compared for different H-NG fuel blends, engine loads and engine leaning (lean-burn operation). The two modelling approaches are studied to capture H-NG combustion in a lean-burn (air-excess ratio higher than 1.6) marine SI natural gas engine. The novelty of this paper is twofold. First, this paper presents an extended heat release rate model based on engine measurements for a zero valve overlap marine (500 kWe) lean-burn SI natural gas engine to account for the impact of large amounts of trapped residual gas on the in-cylinder process. Secondly and more importantly, this paper provides a detailed comparison between the capabilities of Seiliger and double Wiebe function-based model to characterize the H-NG combustion process for varying H-NG fuel blends, engine leaning and engine loads. The developed heat release rate model forms the first step towards the characterization of H-NG combustion using the two modelling approaches. For this research, the simulation model development cycle depicted in Figure 1.1 is followed. The mathematical (conceptual) H-NG combustion models, programmed in Matlab/Simulink, are developed and calibrated by analysis of engine measurements (reality) for the development of high-quality models.

In this paper, the research approach and the test setup are described in Section 2. Section 3 details the 0-D H-NG HRR model developed from engine measurements. Using the outputs of the HRR model, section 3 discusses the development of 0-D Seiliger-based and double Wiebe function-based H-NG combustion characterization models. In section 4, the results of Seiliger and Wiebe modelling approaches are presented for a single test condition and compared with engine measurements. Section 5 provides a detailed comparison of the two modelling approaches in terms of their abilities to characterize and capture the effects of hydrogen

addition, engine leaning (lean-burn operation) and engine load variations on the combustion process. Section 6 presents the research conclusions and recommendations for future work.
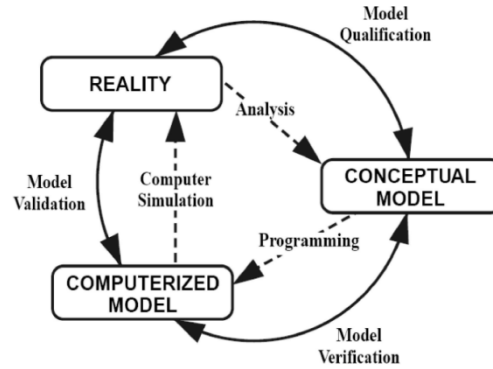
## 2 RESEARCH APPROACH AND TEST SETUP

### 2.1 Research Approach

In this study, H-NG combustion was measured on a 500 kW marine SI natural gas engine by replacing the natural gas with different hydrogen percentages and keeping the total power output constant. Table 2.1 shows the hydrogen-natural gas (H-NG) fuel blends tested, while the test setup and engine specifications have been described in the next subsection.

The engine performance was tested at 90%, 75%, 50% and 25% loads as shown in Table 2.3. It should be noted that it was not possible to study the effects of hydrogen addition at 90% load because of test limitations explained in the subsequent paragraphs. For each combination of H-NG blend and engine load, experiments were also performed at different values of air-excess ratio to control the NOx emissions and study the effects of engine leaning. For this purpose, engine performance was first measured at a fixed load point and NOx value, and then the engine was leaned, by increasing the air-intake (air-excess ratio) via manual control, to a lower value of NOx measured in mg/Nm$^3$ (at 5% reference oxygen). In this manner, engine performance for a fixed H-NG blend and load was measured at different NOx values from 500 mg/Nm$^3$ of NOx to misfire as shown in Table 2.3. The engine was initially leaned in steps of 100 mg/Nm$^3$ of NOx and, then, in steps of 50 mg/nm$^3$ NOx until misfire. For 0H-NG fuel blend and 500 mg/Nm$^3$ of NOx at 75% load, the value of air-excess ratio was higher than 1.6 and increased with engine leaning, thus, representing the lean-burn operation [5].

Table 2.1: Tested Hydrogen-natural gas fuel blends

| Fuel Blends | Natural gas (Volume %) | Hydrogen (Volume %) |
|---|---|---|
| 0H-NG | 100 | 0 |
| 5H-NG | 95 | 5 |
| 10H-NG | 90 | 10 |
| 20H-NG | 80 | 20 |

Figure 2.1 shows the four-step research approach followed for this study. After completing the first step of H-NG engine performance experiments, the heat release rate (HRR) model was derived. Since the heat release cannot be directly measured and is integral to the development of the Seiliger and Wiebe-based combustion models, the in-cylinder pressure and crank angle measurements were used as the inputs for the 0-D, single zone H-NG Heat Release Rate (HRR) model. This model was used to describe the detailed heat release process in the zero valve overlap lean-burn test engine for combustion of different H-NG fuel mixtures at varying engine loads and air-excess ratios (NOx emissions). In the third step, various outputs of the HRR model were used to develop two 0-D combustion characterization models capable of capturing the effects of hydrogen-natural combustion. The first model employed the first-principle, thermodynamic 5-stage Seiliger process modelling to characterize the H-NG combustion process, while in the second model a double Wiebe function was used in a 0-D, single zone model to capture the combustion at every crank angle. In this step, various Seiliger and Wiebe combustion parameters were used to define and characterize H-NG combustion process for different H-NG blends, loads and engine leaning. Lastly, both the combustion characterization models were compared in their capabilities to capture the changes in the combustion process due to hydrogen addition, load variations and engine leaning (lean-burn operation). In this manner, Seiliger and double Wiebe

function-based 0-D combustion models were developed to study and capture the H-NG combustion process in a marine lean-burn SI engine based on engine measurements.
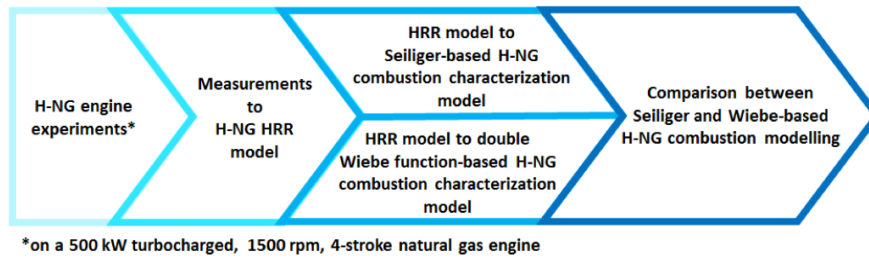


Figure 2.1: Research methodology

In this paper, all the simulation and modelling results are presented at the 500 mg/Nm$^3$ of NOx value (at 5% reference oxygen) unless mentioned otherwise. The 500 mg/Nm$^3$ of NOx value is close to and lower than the NOx IMO TIER-III limit for this engine, which is 2.08 g/kWh. During experiments, the measurements with different hydrogen percentages were restricted to the maximum load set-point of 75% load. This is because, at 90% load and 0H-NG, the engine was operating at its turbocharging limit, i.e., it was not possible to lean out the engine to 500 mg/Nm$^3$ of NOx at 90% load and 5H-NG as the engine had reached its leaning limit.

## 2.2    Test setup

The experiments were performed on an eight-cylinder, turbocharged spark-ignited natural gas engine. Table 2.2 lists the specifications of the test engine with a zero valve overlap and rated power of 500 kWe at 1500 rpm. The test engine was connected to a generator to apply the load at 1500 rpm. In this manner, engine measurements were performed at varying engine loads of 90%, 75%, 50% and 25% at rated rpm. To study the effects of hydrogen addition, natural gas was replaced by 5%, 10% and 20% hydrogen, by volume, at 75%, 50% and 25% engine loading as explained in the above subsection and seen in Table 2.3.

Table 2.2: Engine Specifications

| Parameters | Value/Unit |
|---|---|
| Number of Cylinders | 8 |
| Bore | 0.17 m |
| Stroke | 0.19 m |
| Rated speed | 1500 rpm |
| Rated power | 500 kWe |
| Compression ratio | 12:1 |
| Boost pressure | 2.2 bar |
| Spark Timing | 24$^0$CA BTDC |
| Inlet Valve Open (IO) | 8.7$^0$CA ATDC |
| Exhaust Valve Open (EO) | 20.1$^0$CA BBDC |
| Inlet Valve Close (IC) | 21.5$^0$CA ABDC |
| Exhaust Valve Close (EC) | 11.8$^0$CA BTDC |

Table 2.3: Conditions Tested

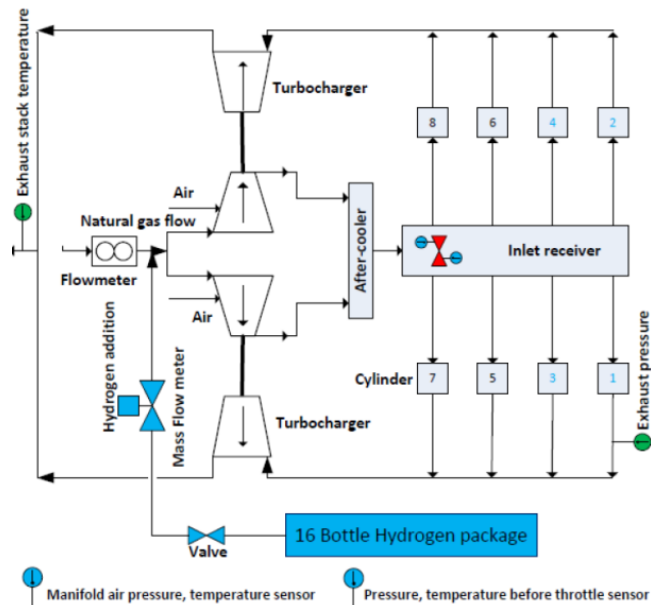| Engine Load [%] | H-NG Blends | NOx [mg/Nm3] |
|---|---|---|
| 90 | 0H-NG | Only 500 |
| 75 | 0, 5, 10, 20H-NG | 500 to misfire |
| 50 | 0, 5, 10, 20H-NG | 500 to misfire |
| 25 | 0, 5, 10, 20H-NG | 500 to misfire |



Figure 2.2: Schematic representation of the test setup [8].

Natural gas flow was injected in the engine before the turbocharger and measured using a flowmeter. Hydrogen stored in pressurized bottles was injected in the natural gas line before the turbocharger, and the flow of hydrogen was controlled via a mass flow meter. During these experiments, temperatures, pressures, and flow rates were measured at different locations within the test setup, which have been depicted in Figure 2.2. For this study, air-intake (air-excess ratio) was varied for each combination of H-NG fuel blend and engine load to measure at different NOx emissions as listed in Table 2.3. A schematic representation of the test setup including the hydrogen addition setup has been presented in Figure 2.2. Cylinders 1, 2, 3 and 4 were equipped with a water-cooled Kistler 7061B sensors for in-cylinder pressure measurements. The sensors were flushed in each cylinder head to record a clean pressure signal. The in-cylinder pressure data was continuously measured in sets of 147 consecutive cycles at each measurement point using the Kistler Ki-Box measurement unit [45]. The average in-cylinder pressure and crank angle measurements were used as a starting point to model the

heat release process for varying hydrogen-natural gas blends, loads and engine leaning. The water-cooled pressure sensor has a sensitivity shift of +/- 0.5% while the charger amplifier used with the sensor for the conversion of electrical charge into voltage has a maximum error of +/- 3% [46]. Considering these two errors, the pressure sensor has a maximum cumulative deviation of +/-3.39% in measurements. The next section describes the zero-dimensional heat release rate and combustion models in detail.

# 3 H-NG ZERO-DIMENSIONAL COMBUSTION MODELLING

## 3.1 Measurements to 0-D Heat Release Rate (HRR) model

To study the heat release process of hydrogen-natural gas (H-NG) fuel blends, a single-zone, 0-D, thermodynamic heat release rate (HRR) model has been developed for hydrogen-natural gas (H-NG) combustion. The building blocks for this heat release rate model are in-cylinder pressure and crank angle measurements. The heat release rate model is the first step towards the characterization of hydrogen-natural gas combustion using the Seiliger and double Wiebe function-based modelling approach based on engine measurements.

The experiments were performed on an engine with zero valve overlap. The absence of valve overlap leads to large amounts of trapped residual gas, which has an impact on the trapped mass, in-cylinder temperature and even heat release. Therefore, it is important to calculate the trapped residual gas. This subsection discusses the heat release rate model while using the engine measurement to account for the amount of trapped residual gas and the impact on the in-cylinder combustion process. The developed H-NG HRR model has been adopted from the HRR model used for diesel combustion [46].

### 3.1.1 Energy balance

The 0-D H-NG HRR model solves the mass, composition and energy balance at every crank angle starting with the trapped condition within the cylinder at the closing of the inlet valve. The first law of thermodynamics is used to compute the combustion reaction rate (CRR) provided in equation 3.1. The term $u_{comb-fuel}$ is the effective heat of combustion and depicts the fuel energy. It is dependent on temperature, composition of the hydrogen-natural gas fuel blend and also the properties of fuel, air and combustion gas [47]. For diesel combustion, the effective heat of combustion value would also include the heat loss due to fuel evaporation [46], however, this evaporation heat loss is disregarded in case of gaseous hydrogen-natural gas fuel combustion.

$$CRR = \frac{\dot{U} + \dot{W} + \dot{Q}_{loss}}{u_{comb-fuel}} = \frac{m.c_v.\dfrac{dT}{dt} + p.\dfrac{dV}{dt} + \dot{Q}_{loss}}{u_{comb-fuel}}$$

3.1

where, $\dot{U}$: internal energy in kJ/sec; $\dot{W}$: work in kJ/sec; $\dot{Q}_{loss}$: heat loss in kJ/sec; dV/dt: rate of volume change; m: in-cylinder mass in kg, $c_v$: specific heat at constant volume in kJ/kgK

In equation 3.1, the pressure (p) is obtained for the in-cylinder pressure measurements, while rate of volume change is calculated as a function of crank-angle [47]. The heat loss to the walls, piston crown and cylinder head is estimated by using the Woschni heat loss formulation for the heat transfer coefficient [46]. The trapped in-cylinder mixture is assumed to be an ideal gas with uniform temperature and pressure within the cylinder [31]. The H-NG HRR model uses the ideal gas law to compute the average in-cylinder mixture temperature (T) during the cycle from the in-cylinder pressure measurement, volume, in-cylinder mass (m) and the mixture gas constant. Since this average in-cylinder temperature is calculated based on measured variables in the HRR model, it is referred to as the measured in-cylinder temperature for all the subsequent sections in this paper. For the temperature estimation, the in-cylinder mass is calculated from the mass balance, while the in-cylinder mixture gas constant ($R_{mixture}$) is computed from the composition balance of the air ($x_{air}$), combustion gas ($x_{cg}$) and fuel ($x_{fuel}$) along with their properties as given by equation 3.2.

$$R_{mixture} = x_{air} \cdot R_{air} + x_{cg} \cdot R_{cg} + x_{fuel} \cdot R_{fuel}$$

3.2

Similar to the gas constant, the specific heat at constant pressure of the mixture is a summation of the in-cylinder composition and the corresponding specific heats of each in-cylinder component (air, combustion gas and fuel). The gas constant is subtracted from the specific heat at constant pressure to obtain the specific heat at constant volume, which is required for internal energy.

7

### 3.1.2  Mass and composition balance

In the test engine, the air and natural gas enter the cylinder as a premixed mixture and combine with the residual gas from the previous cycle. Therefore, the total mass of in-cylinder mixture (m) at any moment within the closed cylinder is a sum of the mass of air ($m_{air}$), mass of combustion gas ($m_{cg}$) and the mass of fuel ($m_f$). The mass of fuel burnt at every crank angle is given by the reaction co-ordinate (RCO), which is obtained by integrating the CRR as given by equation 3.3. Division of RCO by the initial or trapped fuel mass ($m_{f,t}$) gives the normalized reaction co-ordinate ($RCO_{norm}$), which is the fuel mass-burn fraction that monotonously increases from zero to 1. Using the RCO, trapped in-cylinder mass ($m_t$), trapped air fraction ($x_{air,t}$), trapped residual gas fraction ($x_{rg,t}$) and the stoichiometric air-to-fuel ratio ($\sigma$), the model solves the following mass balance at every crank angle to compute the mass of each in-cylinder component.

$$m_f = RCO = \int CRR \qquad\qquad 3.3$$

$$m_{air} = x_{air,t} \cdot m_t - m_f \cdot (\sigma) \qquad\qquad 3.4$$

$$m_{cg} = x_{rg,t} \cdot m_t + m_f \cdot (\sigma + 1) \qquad\qquad 3.5$$

$$m = m_{air} + m_{cg} + m_f \qquad\qquad 3.6$$

The computed mass of each component is used to calculate the corresponding mass fractions (x) and the in-cylinder composition. Equations 3.7 to 3.10 give the composition balance inside the cylinder.

$$x_{air} = \frac{m_{air}}{m} \qquad\qquad 3.7$$

$$x_{cg} = \frac{m_{cg}}{m} \qquad\qquad 3.8$$

$$x_f = \frac{m_f}{m} \qquad\qquad 3.9$$

$$x_{air} + x_{cg} + x_f = 1 \qquad\qquad 3.10$$

To solve the mass balance in equations 3.4 to 3.6, the model needs the trapped in-cylinder mass, trapped air fraction and the trapped residual gas fraction. Trapped mass is estimated by using the ideal gas law given in equation 3.11.

$$m_t = \frac{p_t \cdot V_t}{R_t \cdot T_t} \qquad\qquad 3.11$$

In equation 3.11, the trapped pressure ($P_t$) is obtained from engine measurements and trapped volume ($V_t$) is equal to the cylinder volume at inlet valve closing, which is calculated from the crank angle [47]. The remaining two variables, i.e., the trapped mixture gas constant ($R_t$) and trapped temperature ($T_t$) are derived as follows.

To calculate the gas constant at trapped condition by using equation 3.2, mass fractions of each mixture component are computed. The trapped residual gas fraction is dictated by the valve overlap. The current test engine has no valve overlap since the exhaust valve closes before the opening of the inlet valve as seen from Table 2.2. This zero valve overlap restricts methane slip and scavenging, thus, trapping a good amount of residual combustion gas from the previous cycle at the point of inlet valve closing [23]. The trapped residual gas plays a crucial role in the combustion process to control the in-cylinder temperatures and also the NOx emissions. The amount of trapped residual gas in a zero valve overlap gas engine needs to be taken into account as the mass fraction was found to be higher than 15%. Therefore, the trapped air mass fraction is calculated as a function of the residual gas mass fraction, air-excess ratio ($\lambda$) and the stoichiometric air-to-fuel ratio presented in equation 3.12 [48]. Derivation for equation 3.12 is provided in Appendix 2. After calculating the trapped air fraction, the trapped fuel fraction is obtained from equation 3.10.

$$x_{air,t} = \frac{m_{air,t}}{m_t} = \frac{(1 - x_{rg,t}) \cdot \sigma \cdot \lambda}{\sigma \cdot \lambda + 1} \qquad\qquad 3.12$$

The high amount of trapped residual gas, which is left behind after the exhaust blowdown, increases the temperature of the trapped mixture [23]. During the induction stroke, the induction temperature ($T_{ind}$) of the entering air-fuel mixture will be higher than the measured manifold temperature ($T_{man}$) due to a heat pick-up from the inlet duct walls. Therefore, the final trapped temperature is higher due to the combined effect of the increased induction temperature and mixing with the hot residual combustion gases trapped from the previous

cycle. Equation 3.13 accounts for the combined effect on the trapped temperature. A derivation of the trapped temperature formulation along with the derivation of variables $T_{ind}$, $P_{bld}$ and $T_{bld}$ is presented in Appendix 3.

$$\frac{1}{T_t} = \frac{(V_{IC} - V_{IO})}{V_{IC} \cdot T_{ind}} + \frac{(V_{EC} \cdot P_{bld})}{V_{IC} \cdot P_t \cdot T_{bld}} \qquad 3.13$$

where, $V_{IC}$, $V_{IO}$ and $V_{EC}$: cylinder volumes at inlet valve closing, inlet valve opening and exhaust valve closing, respectively. $P_{bld}$ and $T_{bld}$: pressure and temperature after blowdown when the exhaust valve opens.

In this manner, the trapped mass can be calculated and a correct estimation of the trapped residual gas fraction leads to an accurate estimation of the trapped fuel mass, trapped air mass, mass balance and composition balance that matches with the engine measurements.

### 3.1.3   H-NG HRR model outputs

Using the above-described HRR model, the heat release process is studied for varying percentages of hydrogen-natural gas fuel mixtures and engine loads. For each hydrogen-natural gas blend and at each engine load, the HRR model also simulates the in-cylinder process for engine leaning between 500 mg/Nm³ of NOx and misfire to study the engine performance during leaning. The model uses in-cylinder pressure and crank-angle measurements to compute the mass-burn fraction/normalized reaction co-ordinate, net combustion heat, work output and temperature inside the cylinder at every crank angle. Figure 3.1 shows the average in-cylinder temperature and the $RCO_{norm}$ simulated by the HRR model for 10H-NG fuel blend at 375 kWe and 500 mg/Nm³ of NOx. As seen in the figure below, the average in-cylinder temperature rises with combustion and reaches its maximum value after TDC. The normalized RCO represents the mass-burn fraction of the H-NG fuel as the fuel begins to combust just after the spark is provided at 24 degrees BTDC. After approximately 80% of the mass-burn fraction, the combustion process slows down as it reaches a value of 1 indicating end of combustion.
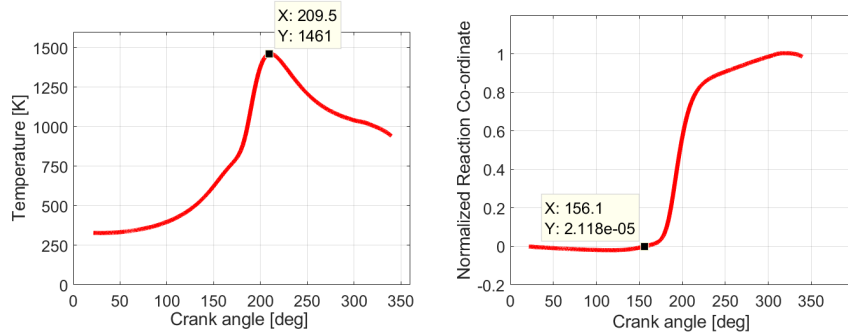


a) In-cylinder temperature versus crank angle          b) Normalized reaction co-ordinate versus crank angle

Figure 3.1: HRR model simulation of average in-cylinder temperature (a) and normalized reaction co-ordinate (b) for 10H-NG fuel blend at 375 kWe load and 500 mg/Nm³ NOx

The HRR model outputs are used further in the combustion characterization models of Seiliger and Wiebe to emulate the combustion of hydrogen-natural gas fuel in the engine. This characterization of H-NG combustion using Seiliger and Wiebe modelling has been discussed in the next subsection.

## 3.2   HRR model to Seiliger-based H-NG combustion characterization model

The Seiliger process uses five stages to thermodynamically describe the in-cylinder process out of which three stages describe the combustion process [37]. The three combustion stages are constant volume or isochoric combustion (2-3), constant pressure or isobaric combustion (3-4) and constant temperature or isothermal combustion (4-5) as shown in Figure 3.2(a). These three stages combined with the polytrophic compression (1-2) and expansion (5-6) processes can be used to compute the temperature, pressure, net combustion heat and work during each stage within the in-cylinder process. Figure 3.2(a) shows the five stages of the Seiliger cycle represented in a pressure-volume diagram. In the Seiliger process, the thermodynamic relationships between each stage can be derived analytically to calculate the pressures (p), volumes (V) and temperatures (T) at the beginning and end of each stage. These analytical correlations are mainly based on three Seiliger combustion parameters, namely, Seiliger parameter 'a', Seiliger parameter 'b' and Seiliger parameter 'c'. The definitions of these Seiliger parameters have been presented in Figure 3.2(a), while the analytical thermodynamic correlations have been presented in Table A4.1 of Appendix 4 [37].

a) Seiliger cycle          b) Outline of Seiliger-based H-NG combustion characterization procedure
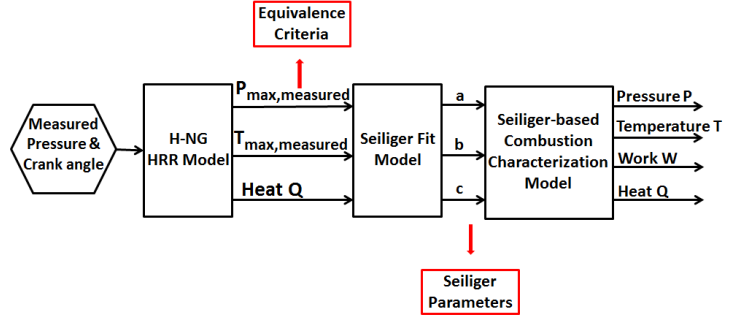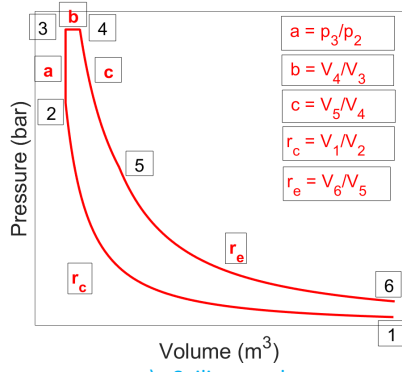
Figure 3.2: Definition of five-stage Seiliger process with in-cylinder pressure-volume diagram (a) and outline of H-NG combustion characterization procedure using the Seiliger process (b)

To characterize the H-NG combustion process using the Seiliger cycle, the Seiliger parameters need to be determined. In this study, the Seiliger parameters are determined from the H-NG HRR model. Figure 3.2(b) shows the outline of the H-NG combustion characterization procedure using the Seiliger cycle. At first, the HRR model is used to capture the heat release process from the in-cylinder pressure measurements for a fixed operating point of load, hydrogen percentage and NOx emission as explained in subsection 3.1. Next, the measured maximum pressure ($p_{max}$) along with the HRR model outputs of maximum temperature ($T_{max}$) and the net combustion heat ($Q_{net}$) are used as equivalence criteria to numerically determine the Seiliger parameters 'a', 'b' and 'c' that fit the H-NG in-cylinder process in a Seiliger cycle. Then, these derived Seiliger parameters are used to compute the temperatures, pressures, work and heat quantities during each stage in the 0-D Seiliger-based characterization model by using the equations given in Table A4.1 and Table A4.2 of Appendix 4. In Table A4.2, the work and heat quantities are made specific by dividing by trapped mass. The summation of work quantities during each stage gives the indicated work produced by the engine per cylinder. Similarly, the summation of heat during the three stages of combustion provides the net combustion heat per cylinder, and the negative heat during the compression and expansion stage indicate the heat loss. The subsequent paragraph explains the Seiliger cycle fitting procedure in more detail.

In order to accurately fit the Seiliger cycle to the real H-NG in-cylinder and combustion process, a set of three equations is solved numerically to determine the 'a', 'b' and 'c' Seiliger parameters. Equations 3.13 to 3.16 depict this set of three equations for maximum pressure ($p_{max,Seiliger}$), maximum temperature ($T_{max,Seiliger}$) and net combustion heat ($q_{net,Seiliger}$) as a function of the Seiliger parameters [37].

$$p_{max,Seiliger} = p_1 \cdot r_c^{n_c} \cdot a \qquad\qquad 3.14$$

$$T_{max,Seiliger} = T_1 \cdot r_c^{n_c-1} \cdot a \cdot b \qquad\qquad 3.15$$

$$q_{net,Seiliger} = q_{23} + q_{34} + q_{45} \qquad\qquad 3.16$$

$$= c_v \cdot T_1 \cdot r_c^{n_c-1} \cdot (a-1) + c_v \cdot T_1 \cdot \gamma \cdot r_c^{n_c-1} \cdot a \cdot (b-1) + c_v \cdot T_1 \cdot (\gamma-1) \cdot r_c^{n_c-1} \cdot a \cdot b \cdot \ln(c)$$

A Newton-Raphson multi-variable root finding method is applied to determine the three Seiliger parameters [38]. This iterative numerical method finds the Seiliger parameters once the following conditions are met.

$$p_{max,measured} - p_{max,Seiliger} < 1 \qquad\qquad 3.17$$

$$T_{max,measured} - T_{max,Seiliger} < 1 \qquad\qquad 3.18$$

$$Q_{net,measured} - Q_{net,Seiliger} < 10 \qquad\qquad 3.19$$

where, $p_{max,measured}$: maximum pressure in bar from the HRR model, $T_{max,measured}$: maximum temperature in K from the HRR model and $Q_{net,measured}$: net combustion heat in kJ from the HRR model.

The Seiliger-based characterization model for H-NG combustion also requires the polytrophic exponents for compression and expansion. The value of polytropic exponent for compression ($n_c$) is determined from the definition of the polytropic process given by equation 3.20. This value of $n_c$ represents heat loss during the compression process when the polytrophic factor for compression ($\eta_{poly,c}$) in equation 3.21 is greater than one as derived in [37]. Similarly, the value of polytropic exponent for expansion ($n_e$) is set such that the polytropic factor for expansion ($\eta_{poly,e}$) in equation 3.22 is less than one and thus, represents heat loss during the expansion process [37].

10

$$n_c = \ln(\frac{P_1}{P_2} / \frac{V_2}{V_1})$$

<div align="right">3.20</div>

$$\eta_{poly,c} = \frac{\gamma - 1}{n_c - 1}$$

<div align="right">3.21</div>

$$\eta_{poly,e} = \frac{n_e - 1}{\gamma - 1}$$

<div align="right">3.22</div>

Following the above-described procedure, a 0-D Seiliger-based H-NG combustion characterization model is developed from engine measurements to capture the H-NG in-cylinder and combustion process for all load, hydrogen percentage and NOx emission variations.

## 3.3   HRR model to Wiebe-based H-NG Combustion Characterization Model

Wiebe modelling uses semi-empirical functions to estimate the combustion process at every crank-angle, while Seiliger modelling is a first-principle, thermodynamic approach for a discretized three-stage representation of the combustion process. Wiebe functions have been used for alternative fuels, advanced combustion and system integration studies of sequential turbocharging and variable geometry turbines with engines [49]–[52]. A single Wiebe function is mathematically defined by three Wiebe coefficients, i.e., a combustion efficiency factor, a shape factor and the combustion duration [29], [30]. The shape factor dictates the shape of combustion or mass-burn fraction. A typical value of the combustion efficiency factor and the shape factor for SI gasoline engines is 5 and 2, respectively [53]. Diaz et. al. [33] used values of 2.8 and 2.4 for the combustion efficiency and shape factor in a single Wiebe function to study the influence of hydrogen-methane blends on the knock occurrence crank angle (KOCA) in a 2kW Cooperative Fuel Research (CRF) Engine. Shivapuji and Dasappa [54] used a single Wiebe function to model the combustion of producer gas in a 28 kWe SI engine and showed that the Wiebe coefficients need to be adapted to capture the in-cylinder pressure variations. Furthermore, Carrera et. al. performed CFD calculations to determine single Wiebe function coefficients as a function of compression ratio, engine speed, air-excess, spark timing and carbon dioxide content to study biogas combustion [34]. Similarly, Rousseau et.al. used air-excess ratio, spark-timing and engine load to compute the single Wiebe function coefficients for combustion characterization of natural gas in a lean-burn SI engine [35]. However, they concluded that the single Wiebe approach failed in accurately reproducing the experimental mass-burn fraction and recommended further studies to test mathematical functions besides Wiebe. In Wiebe-based combustion modelling, the different combustion rates present during different combustion stages are difficult to capture with a single Wiebe function. Therefore, double Wiebe functions are preferred over single Wiebe functions to capture the premixed and the diffusion combustion stages of diesel. Similarly,  the different combustion phases in a SI H-NG engine can be captured using a double-Wiebe function. Therefore, in this subsection, a double Wiebe function is employed in a zero-dimensional, single zone model to characterize the H-NG combustion process for different loads, hydrogen percentages and engine leaning.

The 0-D Wiebe-based H-NG combustion characterization model is an anti-causal model of the H-NG HRR model, which uses a double-Wiebe function to fit the normalized RCO obtained from the HRR model. The Wiebe-based characterization model solves the same mass, composition and energy balance as that presented in subsection 3.1 for the H-NG HRR model. The model computes the in-cylinder temperature by solving equation 3.1, in which the CRR is obtained by differentiating the Wiebe fitted RCO$_{norm}$. The in-cylinder pressure is estimated by using the ideal gas law. Similar to the H-NG HRR model, the heat loss is determined using the Woschni correlation [46], while all the mixture properties are calculated from compositions and temperatures. The outputs of the 0-D Wiebe-based H-NG combustion characterization model are work done and heat released along with average in-cylinder pressures and temperatures at every crank angle.

$$RCO_{norm} = b_1 \cdot (1 - e^{-a_1 \cdot (tau_1)^{(m_1+1)}}) + b_2 \cdot (1 - e^{-a_2 \cdot (tau_2)^{(m_2+1)}})$$

<div align="right">3.23</div>

where, $tau_1 = \dfrac{\theta - SOC}{CD_1}$,      $tau_2 = \dfrac{\theta - SOC}{CD_2}$,      $\theta$: Instantaneous crank-angle in degrees

$$a_1 = a_2 = -\log(1 - \eta_{comb})$$

<div align="right">3.24</div>
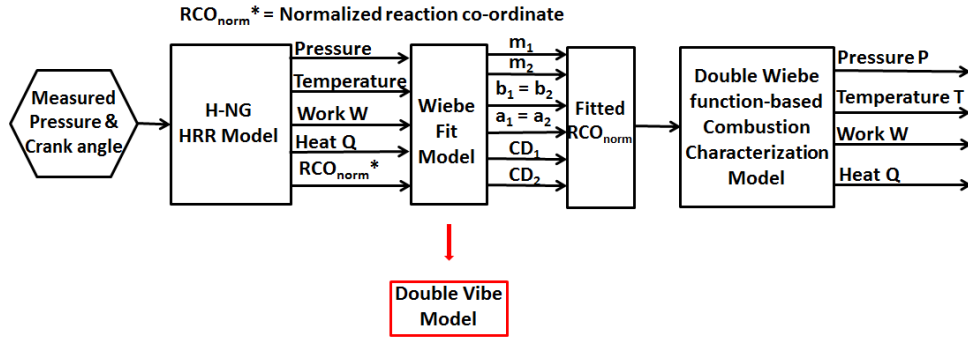
**RCO_norm* = Normalized reaction co-ordinate**

Figure 3.3: Outline of the H-NG combustion characterization procedure using Wiebe modelling

For the Wiebe-based combustion characterization process, the normalized reaction co-ordinate ($RCO_{norm}$) or mass-burn rate obtained from H-NG HRR model is mathematically replicated using a double-Wiebe function. Figure 3.3 shows the outline of the H-NG combustion characterization procedure using Wiebe modelling. Equation 3.23 gives the double Wiebe function used to capture the H-NG combustion process. This double-Wiebe function in its generalized form uses eight parameters ($a_1$, $a_2$, $b_1$, $b_2$, $m_1$, $m_2$, $CD_1$ and $CD_2$) to characterize the combustion process. However, this function can be further simplified to reduce the number of independent parameters. In this double-Wiebe function, $b_1$ and $b_2$ are weighing factors defining the fraction of combustion process determined by each Wiebe function. These values are fixed at $b_1$ equal to 0.8 and $b_2$ equal to $1 - b_1$ or 0.2, as the first Wiebe function is able to capture the combustion process till about 80% of mass-burn fraction, while the remaining 20% is estimated by the second Wiebe function. The parameters $a_1$ and $a_2$ are equal and a function of combustion efficiency as given in equation 3.24. The combustion efficiency ($\eta_{comb}$) is determined by calculating the conversion rate of the carbon from the fuel to carbon dioxide. Thus, the combustion efficiency is estimated by dividing the carbon atoms in the exhaust carbon dioxide to the number of carbon atoms that are present in the incoming hydrogen-natural gas blend [8]. In this manner, four out of eight parameters in equation 3.23 are fixed and can be easily determined. Out of the remaining four combustion parameters, $CD_2$ is the combustion duration from the start of combustion (SOC) to end of combustion (EOC), i.e., when the normalized RCO from the HRR model reaches unity. $CD_1$ is the combustion duration from the start of combustion to 80% of mass-burn fraction while the parameters $m_1$ and $m_2$ are commonly referred to as the combustion shape or form factor [29], [55]. The second Wiebe function in equation 3.23, is used to capture the late burn phenomenon observed in the final stage of combustion as shown in Figure 3.1(b) and Figure 3.4. This phenomenon of late combustion was also reported by Rousseau et.al. [35], and confirmed by Ishii et.al. [56] as they continuously detected light emissions by a sensor located in the cylinder head. A least-square fit method is used for the determination of the Wiebe combustion parameters $m_1$, $m_2$ and $CD_1$ to fit the double-Wiebe function to the measured normalized RCO from the H-NG HRR model. In this paper, the primary combustion phase is a combination of the flame-development phase (spark-discharge to 10% mass-burn fraction) and the flame-propagation phase (rapid-burning phase) found in SI engines [31]. The flame-termination or the after-burning phase is analogous to the late combustion discussed in this paper.
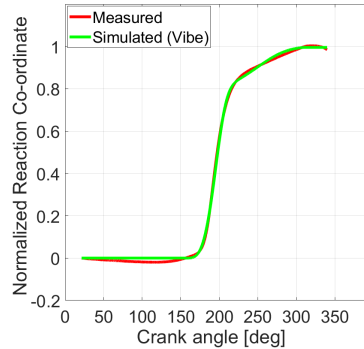


Figure 3.4: Comparison between measured (HRR) and simulated (Wiebe) normalized reaction co-ordinate for 10H-NG fuel blend at 75% engine load and 500 mg/Nm$^3$ of NOx

Figure 3.4 shows the comparison between the measured normalized RCO from the H-NG HRR model and the mass-burn fraction estimated by the double-Wiebe function at 75% load for 10H-NG fuel blend at 500 mg/Nm$^3$ of NOx (at 5% reference oxygen). As shown in Figure 3.4, the simulated RCO by the double-Wiebe function

satisfactorily captures the fuel combustion rate inside the cylinder from SOC to 80% mass-burn fraction and then from 80% mass-burn fraction to EOC as the combustion process slows down.

Following the above-described procedure, a 0-D Wiebe-based H-NG combustion characterization model is developed from engine measurements to capture the H-NG in-cylinder and combustion process for all load, hydrogen percentage and engine leaning (air-excess ratio/NOx emission) variations.

# 4 MODELLING RESULTS

In this section, simulation results from the 0-D Seiliger and double Wiebe function–based combustion characterization models are compared against engine measurements for a single test condition. Additionally, values of Seiliger and Wiebe combustion parameters derived from the characterization process for different H-NG fuel blends and engine leaning or lean-burn combustion have been presented. A detailed discussion on the capabilities of both the models to capture the H-NG combustion process using these combustion parameters has been provided in section 5.

## 4.1 Characterization of H-NG combustion using Seiliger modelling

After determining the Seiliger parameters and polytropic exponents, the Seiliger cycle can be used to capture the H-NG in-cylinder process using the equations in Table A4.1 and Table A4.2 of Appendix 4. These equations combined form the Seiliger-based combustion characterization model present in Figure 3.2(b). Figure 4.1 shows the comparison between the measured and simulated in-cylinder pressures and temperatures using the Seiliger-based combustion characterization model for 10H-NG fuel blend at 75% engine load and 500 mg/Nm$^3$ of NOx. As seen in Figure 4.1 and Table 4.2, the Seiliger process is able to perfectly capture the H-NG in-cylinder process with an accurate estimation of pressures, temperatures, net combustion heat and indicated work output. Table 4.1 provides derived values of the Seiliger parameters and polytropic exponents for the tested condition. The error percentages between the Seiliger model simulation values and the measured values for these performance parameters are very small as shown in Table 4.2.

Table 4.1: Seiliger parameters & polytropic exponents for 10H-NG fuel blend at 75% engine load & 500 mg/Nm$^3$ NOx

| a | b | c | $n_c$ | $n_e$ |
|---|---|---|---|---|
| 1.416 | 1.387 | 1.765 | 1.332 | 1.297 |

Table 4.2: Error between the Seiliger combustion characterization simulation & measured values of performance parameters for 10H-NG fuel blend at 75% engine load & 500 mg/Nm3 NOx

| Parameters | $p_{max}$ | $T_{max}$ | Work | Net combustion heat | $p_6$ | $T_6$ |
|---|---|---|---|---|---|---|
| Error % | 0 | -2.8e-05 | -0.525 | 1.59e-04 | -2.46 | -2.436 |
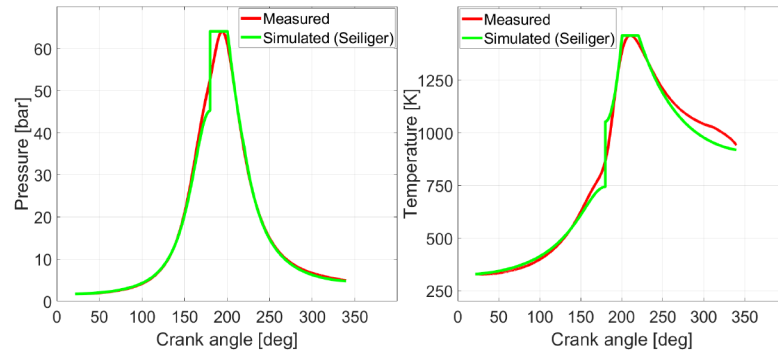


a) In-cylinder pressure versus crank angle     b) In-cylinder temperature versus crank angle

Figure 4.1: Comparison between measured and simulated (Seiliger) in-cylinder pressure (a) and in-cylinder temperature (b) for 10H-NG fuel blend at 75% engine load and 500 mg/Nm$^3$ of NOx

The above-demonstrated capability of the Seiliger-based modelling to accurately estimate the performance parameters is crucial in order to capture the effects of H-NG combustion since hydrogen addition and engine leaning have a direct effect on the peak pressures and temperatures. It is also important to accurately compute the work done and net combustion heat as these parameters are direct indicators of engine performance.

Table 4.3: Combustion heat ratios and Seiliger parameters for different H-NG fuel blends (0H-NG, 10H-NG) and NOx values (500 mg/Nm$^3$, 250 mg/Nm$^3$ of NOx) at 75% engine load

| | $Q_{23,ratio}$ | $Q_{34,ratio}$ | $Q_{45,ratio}$ | a | b | c |
|---|---|---|---|---|---|---|
| NG @ 500 mg/Nm$^3$ NOx | 0.2279 | 0.5427 | 0.2294 | 1.3639 | 1.4522 | 1.7917 |
| 10H-NG @ 500 mg/Nm$^3$ NOx | 0.2703 | 0.5008 | 0.2289 | 1.4162 | 1.3870 | 1.7651 |
| NG @ 250 mg/Nm$^3$ NOx | 0.1298 | 0.5768 | 0.2934 | 1.2045 | 1.5374 | 2.1647 |
| 10H-NG @ 250 mg/Nm$^3$ NOx | 0.1447 | 0.5717 | 0.2836 | 1.2195 | 1.5057 | 2.0655 |

To study and capture the variations in H-NG combustion and in-cylinder process, the Seiliger-based characterization process is used to simulate the combustion process for 0H-NG and 10H-NG fuel blends corresponding to 500 mg/Nm$^3$ and 250 mg/Nm$^3$ of NOx at 75% load. The effects of hydrogen addition and engine leaning on the combustion process are understood by analysing the corresponding heat ratios and the 'a', 'b' and 'c' Seiliger parameters provided in Table 4.3. These simulated heat ratios are an indicator of the amount of heat released during each Seiliger combustion stage and are computed by dividing the combustion heat during a stage by the net combustion heat. The capability of Seiliger-based modelling to capture the shape and stability of the combustion process due to hydrogen addition and engine leaning has been discussed in section 5 by studying the variations in the combustion parameters and heat ratios listed in Table 4.3.

## 4.2 Characterization of H-NG combustion using Wiebe modelling

The ability of the 0-D Wiebe-based combustion characterization model to simulate the in-cylinder pressures and temperatures is demonstrated in Figure 4.2. It compares the measured in-cylinder pressures and temperatures from the H-NG HRR model to the ones computed by the Wiebe-based combustion characterization model for 10H-NG blend at 75% engine load. Furthermore, Table 4.4 provides the derived values of the Wiebe parameters for the same operating conditions, while Table 4.5 shows the error percentages between the measured and the simulated values for various performance parameters using the Wiebe-based H-NG combustion characterization model.

Table 4.4: Derived Wiebe parameters for 10H-NG fuel blend at 75% engine load and 500 mg/Nm$^3$ of NOx

| $m_1$ | $m_2$ | $CD_1$ | $CD_2$ | $\eta_{comb}$ |
|-------|-------|--------|--------|---------------|
| 2.78  | 2.41  | 60.68  | 153    | 0.9777        |

Table 4.5: Error percentages between the simulated (Wiebe) and measured values of performance parameters for 10H-NG fuel blend at 75% engine load and 500 mg/Nm$^3$ of NOx

| Parameters | $p_{max}$ | $T_{max}$ | Work  | Net combustion heat | $p_6$ | $T_6$ |
|------------|-----------|-----------|-------|---------------------|-------|-------|
| Error %    | -1.5      | 0.68      | -5.08 | -2.4                | -1.84 | 0.26  |
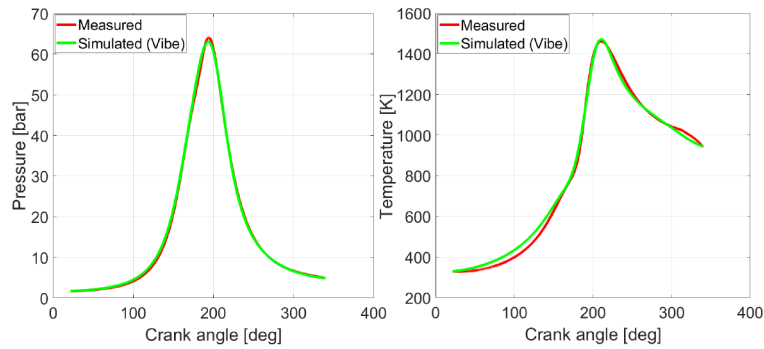


a)  In-cylinder pressure versus crank angle     b)  In-cylinder temperature versus crank angle

Figure 4.2: Comparison between measured and simulated (Wiebe) in-cylinder pressure (a) and in-cylinder temperature (b) for 10H-NG fuel blend at 75% engine load and 500 mg/Nm$^3$ of NOx

As seen in Table 4.5, the errors between measured and simulated H-NG in-cylinder pressures and temperatures using the double Wiebe function are small and similar to those obtained from the Seiliger characterization process. However, unlike Seiliger, the error between simulated and measured work output is high. This is because work is calculated from the simulated in-cylinder pressure shown in Figure 4.2(a), which is dependent on the accuracy of determining the normalized RCO using the double Wiebe function. A small deviation between the measured RCO$_{norm}$ from the H-NG HRR model and the fitted RCO$_{norm}$ can produce errors in simulated work and heat. The accuracy of fitted RCO$_{norm}$ depends on the estimation of Wiebe combustion parameters. Section 5 discusses the deviations and challenges in the estimation of Wiebe combustion parameters for different H-NG fuel blends, engine leaning and loads. Besides Wiebe combustion parameters, deviations in heat loss estimation also contribute to the error in the prediction of work output and also combustion heat. Although the error in prediction of net combustion heat using the Wiebe modelling approach is higher compared to the Seiliger process approach, it is a small deviation. Accurate estimation of work and combustion heat is of high significance since work and heat are main indicators of engine performance and hence, the engine efficiency [46].

| | $m_1$ | $m_2$ | $CD_1$ | $CD_2$ |
|---|---|---|---|---|
| NG @ 500 mg/Nm$^3$ NOx | 2.91 | 2.68 | 62.27 | 149.8 |
| 10H-NG @ 500 mg/Nm$^3$ NOx | 2.78 | 2.41 | 60.68 | 153 |
| NG @ 250 mg/Nm$^3$ NOx | 2.71 | 4.4 | 69.4 | 139 |
| 10H-NG @ 250 mg/Nm$^3$ NOx | 2.75 | 2.86 | 67.17 | 150 |

Similar to the Seiliger-based modelling, the Wiebe-based combustion characterization process is used to study the variations in the H-NG in-cylinder combustion process. Simulations are performed for the same 0H-NG and 10H-NG fuel blends with engine leaning as described in subsection 4.1. Table 4.6 presents the values of Wiebe combustion parameters for each test case. The effects of hydrogen addition and engine leaning are understood by studying the variations in combustion duration and shape parameters, which have been discussed in section 5.

# 5 COMPARISON OF SEILIGER AND DOUBLE WIEBE FUNCTION-BASED MODELLING OF H-NG COMBUSTION

The previous section compared the simulation results of Seiliger and Wiebe modelling approaches against engine measurements for 10H-NG fuel blend at 75% engine load and 500 mg/Nm$^3$ of NOx. In this section, the Seiliger and double Wiebe function-based combustion characterisation models are first compared and studied in terms of their ability to capture the H-NG combustion process for different H-NG fuel blends and engine leaning or lean-burn operation. Then, the models are compared to capture the effects of H-NG combustion at different loads.

## 5.1 Effects of different H-NG fuel blends and lean-burn operation

In section 4, values of Seiliger and Wiebe combustion parameters derived for different H-NG fuel blends (0H-NG, 10H-NG) and engine leaning (500 mg/Nm$^3$, 250 mg/Nm$^3$ of NOx) at 75% engine load were presented. In this sub-section, the derived combustion parameters are used in the combustion characterization models to simulate the H-NG combustion and in-cylinder process. The simulation results from the two modelling approaches are compared against measurements. Moreover, the capabilities of these to modelling approaches to capture the effects of different hydrogen blend percentages and engine leaning are also compared.

### 5.1.1 Seiliger-based H-NG combustion modelling approach

Figure 5.1(a) shows the in-cylinder pressure variations captured by Seiliger process due to increasing hydrogen percentage and decreasing NOx emissions indicating engine leaning. By zooming around the maximum pressure values, the ability of the Seiliger process to capture the minor but important in-cylinder pressure variations relative to the crank angle can be seen in Figure 5.1(b). Similarly, Figure 5.2(a) depicts the in-cylinder temperature variations at 75% load for 0H-NG and 10H-NG fuel blends at 500 mg/Nm$^3$ and 250 mg/Nm$^3$ of NOx, while Figure 5.2(b) zooms into the in-cylinder variations around the maximum temperatures. The variations in the H-NG combustion process are studied by analysing the Seiliger heat ratios and Seiliger combustion parameters provided in Table 4.3. Division of net combustion heat in three Seiliger stages can help capture the shape and stability of the combustion process due to hydrogen addition and engine leaning.

The eight times higher flame speed of hydrogen compared to natural gas, increases the combustion rate and decreases combustion duration [10], [57]. This increase in combustion rate is captured by the increase in Seiliger heat ratio at constant volume ($Q_{23,ratio}$). It increases with an increase in hydrogen percentage as shown in Table 4.3 and signifies faster combustion at constant volume. Increment in $Q_{23,ratio}$ leads to a higher value of Seiliger parameter 'a' and also maximum pressure as depicted in Table 4.3 and Figure 5.1. This increase in combustion heat at constant volume is analogous to the combustion of gasoline that burns instantaneously to release heat at constant volume and is commonly referred to as the Otto-cycle [58]. On the other hand, the $Q_{23,ratio}$ drops along with the Seiliger parameter 'a' as the engine is leaned out to a lower NOx value of 250 mg/Nm$^3$. The resulting decrease in the maximum pressure and temperature values is evident from Table 4.3, Figure 5.1 and Figure 5.2. The depreciation in the value of $Q_{23,ratio}$ due to engine leaning corresponds to the depreciation in combustion rate due to the dilution of incoming charge at higher air-excess ratios. This dilution of fuel charge indicates an increase in combustion instability and cycle-to-cycle variations as explained in [59], [60]. The combustion instability due to engine leaning is manifested in the Seiliger process by a higher value of Seiliger parameter 'b' and a higher combustion heat release at constant pressure ($Q_{34,ratio}$). Table 4.3 and Figure

5.1(b) clearly show that the value of 'b' and $Q_{34,ratio}$ increase as the engine is leaned to decrease the NOx values.



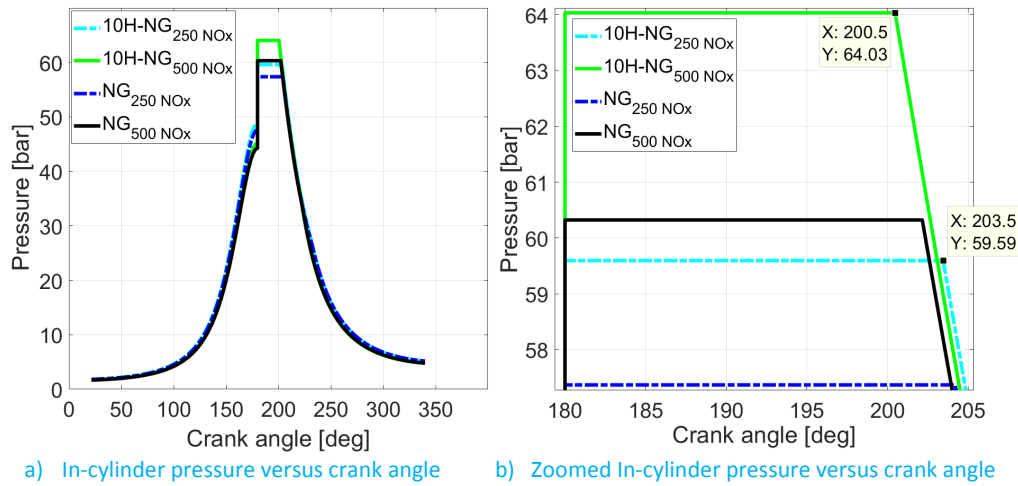a)  In-cylinder pressure versus crank angle          b)  Zoomed In-cylinder pressure versus crank angle

Figure 5.1: In-cylinder pressure variations using the Seiliger-based characterization for different H-NG fuel blends (0H-NG, 10H-NG) and NOx values (500 mg/Nm$^3$, 250 mg/Nm$^3$ of NOx) at 75% engine load

Contrary to engine leaning, hydrogen addition decreases the Seiliger parameter 'b' and also the $Q_{34,ratio}$, thus, representing the increase in combustion stability due to improved combustion rate. Besides 'b', Seiliger parameter 'c' can also help understand combustion stability. An increased value of 'c' in H-NG combustion symbolises reduction in combustion rate and increased late combustion due to engine leaning (lean-burn operation) as more combustion heat is released into the expansion stroke at a constant temperature (higher $Q_{45,ratio}$). The decrease in combustion rate causes the combustion duration to increase, which pushes the point of peak temperature further into the expansion stroke. Thus, engine leaning to 250 mg/Nm$^3$ of NOx not only decreases the peak temperature but also shifts it by about 10 CA degrees into the expansion stroke as seen in Figure 5.2(b). An even lower value of 'a' along with higher values of 'b' and 'c' would be indicative of engine misfire during steady-state operation, which causes the cyclic variations to increase drastically as explained in [61], [62]. Thus, Seiliger parameters 'a', 'b' and 'c' represent different physical phenomenon in the H-NG combustion process.



a)  In-cylinder temperature versus crank angle          b)  Zoomed In-cylinder temperature versus crank angle
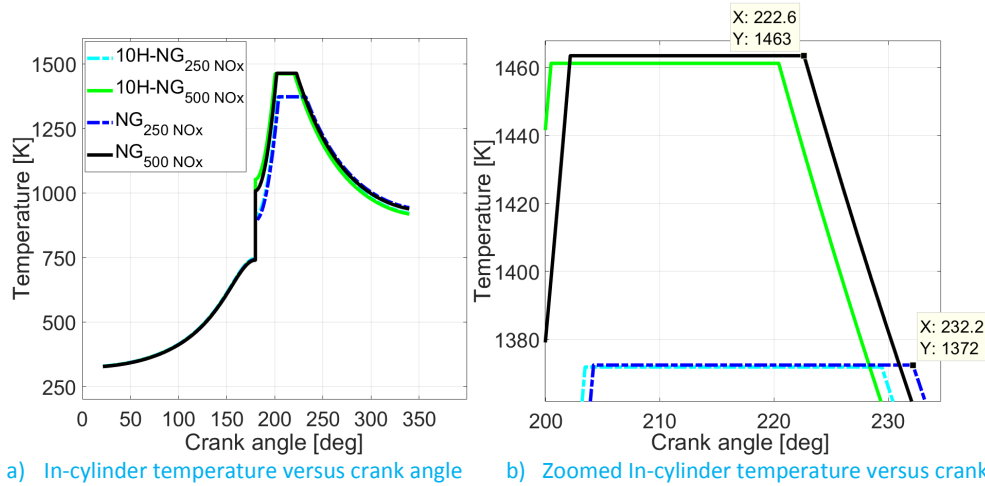
Figure 5.2: In-cylinder temperature variations using the Seiliger process characterization for different H-NG fuel blends (0H-NG, 10H-NG) and NOx values (500 mg/Nm$^3$, 250 mg/Nm$^3$ of NOx) at 75% engine load

During this study of H-NG combustion process, it was also found that the maximum temperatures do not show an excessive increase with hydrogen addition as shown in Figure 5.2. This finding is contrary to the common understanding of hydrogen directly increasing in-cylinder temperatures [63] and can be explained in the following manner. NOx emissions depend on three factors, namely, engine speed, air intake and in-cylinder temperatures [64]–[66]. Since the engine speed is kept constant during these experiments, NOx emissions at a load point are dependent on the air intake and in-cylinder temperatures. During experiments, the air intake is continuously controlled to measure engine performance at the same NOx for all H-NG fuel blends, thus, directly linking NOx emission values to in-cylinder temperatures. Therefore, as the air-intake is controlled, the

16

engine produces almost similar values of maximum in-cylinder temperatures to produce the same amount of NOx emissions. The maximum increase in the peak in-cylinder temperature due to hydrogen addition at 500 mg/Nm$^3$ of NOx was less than 3% of only natural gas performance at all loads. Figure 5.2 also shows that for a decreased NOx value of 250mg/Nm$^3$, the in-cylinder temperatures decreased for 0H-NG and 10H-NG fuel blends. Therefore, combustion due to hydrogen addition can be controlled by governing the air-intake to control the maximum in-cylinder temperatures for NOx production below the IMO TIER-III NOx emission limits.

In this manner, the Seiliger parameters 'a', 'b' and 'c' can be used to accurately characterize the H-NG combustion process and capture the effects of hydrogen addition and engine leaning or lean-burn combustion. Table 5.1 shows the error percentages between the simulation values and the measured values for various performance parameters. As seen from Table 5.1, Seiliger-based approach simulates the combustion process with minor deviations from measured values.

Table 5.1: Error percentages between the Seiliger combustion characterization simulation & measured values of performance parameters for different H-NG fuel blends (0H-NG, 10H-NG) and NOx values (500 mg/Nm$^3$, 250 mg/Nm$^3$ of NOx) at 75% engine load

|  | $p_{max}$ | $T_{max}$ | Work | Net combustion heat | $p_6$ | $T_6$ |
|---|---|---|---|---|---|---|
| NG @ 500 mg/Nm$^3$ NOx, 75% load | 0 | 2.2e-05 | -0.584 | 2.38e-04 | -2.28 | -2.27 |
| 10H-NG @ 500 mg/Nm$^3$ NOx, 75% load | 0 | -2.8e-05 | -0.525 | 1.59e-04 | -2.45 | -2.44 |
| NG @ 250 mg/Nm$^3$ NOx, 75% load | 0 | 1.92e-06 | 0.139 | 3.27e-05 | -2.55 | -2.54 |
| 10H-NG @ 250 mg/Nm$^3$ NOx, 75% load | 0 | -7.6e-05 | -0.012 | 5.06e-05 | -2.66 | -2.64 |

## 5.1.2 Double Wiebe function-based H-NG combustion modelling approach

To understand the variations in the H-NG in-cylinder combustion process, simulation results from the Wiebe-based combustion characterization model have been presented for the same 0H-NG and 10H-NG fuel blends with engine leaning as described in subsection 5.1.1 for Seiliger-based characterization. The effects of hydrogen addition and engine leaning can be well understood by studying the variations in combustion duration and shape parameters provided in Table 4.6 for each test case, while the normalized RCOs are shown in Figure 5.3.

With an increasing percentage of hydrogen in fuel blend, the flame speed of air-fuel mixture increases. This increased flame speed increases the combustion rate. The increase in combustion rate is evident from the increasing steepness of the RCO$_{norm}$ for 10H-NG fuel blends compared to 0H-NG blends in Figure 5.3. This increase in RCO$_{norm}$ with increasing hydrogen percentage is distinctly visible after zooming in around 80% RCO$_{norm}$ as shown in Figure 5.3(b). Contrary to hydrogen addition, engine leaning decreased the slope of RCO$_{norm}$, thus, depicting the deceleration in combustion rate due to charge dilution. The effects of hydrogen addition are also clear from the decreasing value of CD$_1$ shown in Table 4.6 for increasing hydrogen percentage. As expected, CD$_1$ increases with decreasing NOx depicting engine leaning. However, CD$_2$ representing the end phase of the combustion process does not seem to follow the expected and same trend as CD$_1$. This can be explained by the difficulty in accurately determining and understanding the shape of end of combustion and the exact end of combustion as discussed by Heywood [31]. This is could be due to deviations in accurate measurements of in-cylinder pressure-time signals plus the difficulty in accurate estimation of the time-varying heat loss to the cylinder walls, cylinder head and piston crown [31], [35]. Therefore, although the double Wiebe function is able to capture the variations in pressures, temperatures and reaction co-ordinate during the H-NG combustion process, it reached its limitations in precisely defining the H-NG combustion process due to unexpected variations in the combustion duration of the second Wiebe function representing the late burn stage (CD$_2$). The unexpected variations of CD$_2$ are also found for other H-NG fuel blends and are further discussed in subsection 5.2.2. In addition to combustion duration, m$_1$ and m$_2$ are combustion shape parameters, which respectively define the primary combustion phase till 80% mass-burn fraction and the late burn phase represented by the remaining 20%. The primary and late burn stages of the combustion process can be seen for varying H-NG fuel blends and NOx values in Figure 5.4, which depicts the variations in non-dimensional combustion rate or non-dimensional heat release rate.

Table 4.6 and Figure 5.4 show that although the variations in the primary combustion phase with hydrogen addition and engine leaning are small, m$_2$ clearly decreases with increasing hydrogen percentage and increases with engine leaning. An increasing value of m$_2$ with engine leaning or increased lean-burn combustion signifies a deterioration of the combustion process as an increasing amount of heat is released during late combustion. Thus, charge dilution is accompanied by a small increase in heat release late into the expansion stroke. This late burn phase present in lean-burn combustion increases with increasing engine leaning as seen in Figure 5.4(a). Additional discussion on m$_2$ representing an increase in heat release during the late burn combustion phase has been presented in Appendix 5. Conversely, hydrogen decreases the late burn phenomenon with a decreasing

$m_2$. A combination of these Wiebe shape parameters and combustion duration dictates the final variations in in-cylinder pressures and temperatures as shown in Figure 5.5(a) and Figure 5.5(b) respectively. The increase in maximum pressure due to hydrogen addition can be attributed mainly to the decrease in combustion duration for the primary combustion phase ($CD_1$) and the relatively faster heat release depicted in Figure 5.4(b). Even though the maximum values of the non-dimensional combustion rate or non-dimensional heat release rate shown in Figure 5.4 are approximately the same. Similarly, the maximum pressure decreases with engine leaning as $CD_1$ increases and the heat release slows down reaching a lower maximum value. This maximum value of heat release is further shifted into the expansion stroke as depicted in Figure 5.4(b).
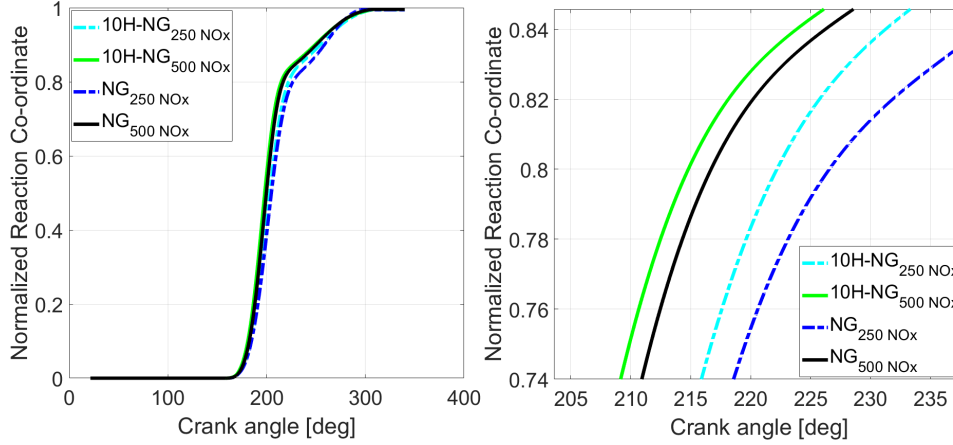


a)  Normalized reaction co-ordinate         b)  Zoomed Normalized reaction co-ordinate

Figure 5.3: Normalized reaction co-ordinate variations using the Wiebe modelling characterization for different H-NG fuel blends (0H-NG, 10H-NG) and NOx values (500 mg/Nm$^3$, 250 mg/Nm$^3$ of NOx) at 75% engine load
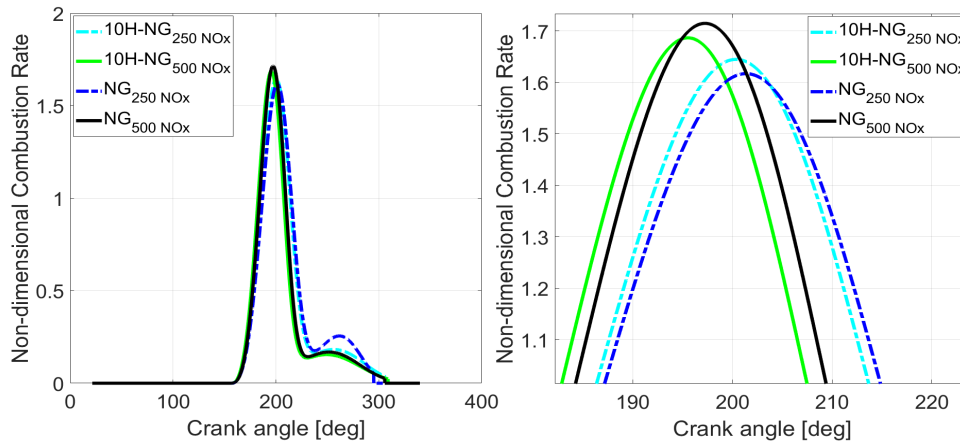


a)  Non-dimensional combustion rate          b)  Zoomed Non-dimensional combustion rate

Figure 5.4: Non-dimensional combustion rate variations using the Wiebe modelling characterization for different H-NG fuel blends (0H-NG, 10H-NG) and NOx values (500 mg/Nm$^3$, 250 mg/Nm$^3$ of NOx) at 75% engine load

Furthermore, as explained earlier in subsection 5.1.1, the maximum in-cylinder temperatures are controlled to produce the same NOx value by controlling the air-intake with hydrogen addition. The temperatures distinctly decrease and retard into the expansion stroke with increased lean-burn operation. These effects on in-cylinder pressure and temperature variations match perfectly to those found using the Seiliger process characterization. However, Wiebe-based characterization showed higher errors between the simulated and measured values of performance parameters as seen from Table 5.2. The maximum error was found to be around 5% for computed work, while combustion heat deviated from measured value by 2.4% at maximum. These higher errors found for Wiebe-based characterization are further discussed in subsection 5.2.2. In this manner, the Wiebe modelling approach is used to characterize the H-NG combustion process by using two combustion shape parameters and combustion durations of a double Wiebe function to define the primary combustion and the late burn combustion stage. The double Wiebe function is also able to capture the changes in late burn phase found in lean-burn NG and H-NG combustion.
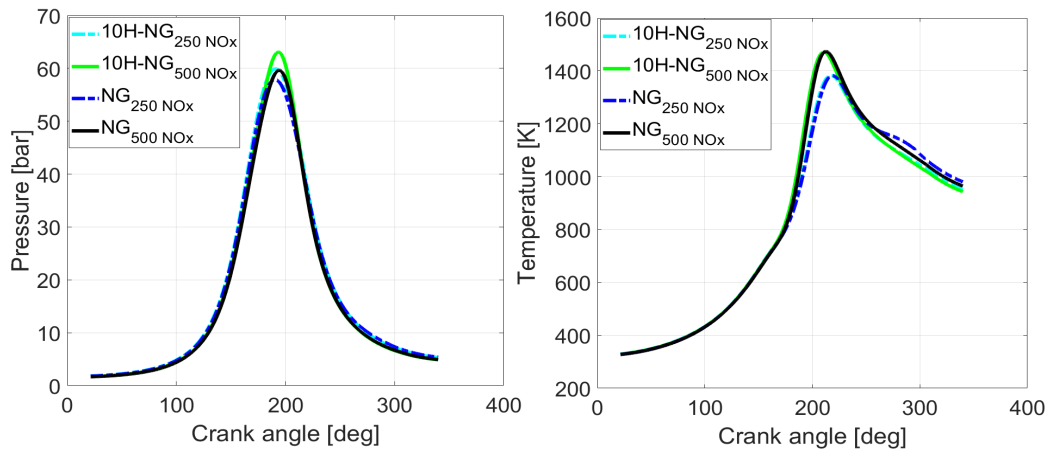
a) In-cylinder pressure versus crank angle      b) In-cylinder temperature versus crank angle

Figure 5.5: In-cylinder pressure and temperature variations using Wiebe characterization process for different H-NG fuel blends (0H-NG, 10H-NG) and NOx values (500 mg/Nm$^3$, 250 mg/Nm$^3$ of NOx) at 75% engine load

Table 5.2: Error percentages between the Wiebe-based combustion characterization simulation & measured values of performance parameters for different H-NG fuel blends (0H-NG, 10H-NG) and NOx values (500 mg/Nm$^3$, 250 mg/Nm$^3$ of NOx) at 75% engine load

| | $p_{max}$ | $T_{max}$ | Work | Net combustion heat | $p_6$ | $T_6$ |
|---|---|---|---|---|---|---|
| NG @ 500 mg/Nm$^3$ NOx, 75% load | -1.17 | 0.67 | -4.72 | -1.98 | 0.5 | 0.5 |
| 10H-NG @ 500 mg/Nm$^3$ NOx, 75% load | -1.5 | 0.68 | -5.08 | -2.4 | 0.24 | 0.25 |
| NG @ 250 mg/Nm$^3$ NOx, 75% load | 0.85 | 0.69 | -4.16 | -0.85 | 1.34 | 1.35 |
| 10H-NG @ 250 mg/Nm$^3$ NOx, 75% load | 0.54 | 0.81 | -4.72 | -1.89 | 0.51 | 0.52 |

In this section, Seiliger and Wiebe modelling approaches were compared in terms of their ability to characterize and capture the H-NG combustion process for different hydrogen percentages and engine leaning. The Seiliger characterization process was able to accurately capture the variations in H-NG in-cylinder process over five discretized stages. Similarly, the Wiebe-based characterization was also able to effectively capture the variations in in-cylinder pressures and temperatures at every crank angle. However, it reached its limitations in precisely capturing the H-NG combustion process due to unexpected variations in the combustion duration of the second Wiebe function defining the late burn stage. Additionally, Wiebe-based characterization also produced larger errors in the estimation of work output. Both Wiebe and Seiliger modelling approaches showed that the addition of hydrogen strengthens combustion stability. The increase in combustion stability was depicted in Wiebe modelling by the increased combustion rate or the decreased combustion duration ($CD_1$) and late combustion. The enhanced stability was also depicted via the Seiliger modelling approach by the increase in Seiliger parameter 'a' and the decrease in Seiliger parameters 'b' and 'c'. This enhanced combustion stability due to hydrogen addition allows engine leaning to higher air-excess ratios, which expands the operating window between the IMO TIER-III NOx limit (500 mg/Nm$^3$ at 5% reference $O_2$) and misfire in comparison to only natural gas marine engines [6].

In this paper, $p_{max}$, $T_{max}$, work, net combustion heat, $p_6$ and $T_6$ modelling parameters are presented for the purpose of comparison between the two modelling approaches as these variables are vital for investigating system integration, controls and load variations. Additionally, these performance variables are the common parameters that can be obtained directly from both the modelling approaches as shown in Table A1.1 of Appendix 1. Therefore, these parameters can be studied to compare the capabilities of the Seiliger and Wiebe modelling approach in capturing the H-NG in-cylinder and combustion process. Other crank-resolved parameters such as CA10, CA50, CA90, corresponding pressures, and temperatures along with the maximum rate of pressure rise can also be important parameters for combustion analysis. Appendix 1 provides a discussion about the estimation of these parameters for 20H-NG fuel blend at 75% engine load and 500 mg/Nm$^3$ of NOx using the Seiliger and Wiebe modelling approaches.

## 5.2    Effects of different H-NG fuel blends and engine loads

To study the effects of hydrogen addition at a fixed engine load, first, the engine was controlled to operate at a fixed NOx with only natural gas fuel. Next, hydrogen was added to replace a fixed volumetric percentage of natural gas flow while controlling the air-intake to produce the same NOx value and the same engine load. This led to a decrease in the incoming natural gas flow with an increase in air-excess ratio compared to the initial or benchmark case of only natural gas operation. Therefore, at a fixed engine load and NOx value, all the effects

of hydrogen addition on engine performance could be understood as deviations from the benchmark performance of the engine operating on only natural gas. In this section, the H-NG combustion process is studied in terms of deviations in Seiliger and Wiebe combustion parameters for different hydrogen blend percentages and engine loads at a fixed NOx of 500 mg/Nm$^3$ (at 5% reference $O_2$). The trends of combustion parameters for both the modelling approaches are discussed to understand their capabilities and limitations in capturing H-NG combustion process over the engine load range. The values of performance parameters simulated for different engine loads by the two combustion characterization modelling approaches are compared with measured values.

In order to understand the deviations in combustion parameters, first, the combustion parameters are computed for all H-NG fuel blends (5H-NG, 10H-NG and 20H-NG) and engine loads by applying the combustion characterization approaches for Seiliger and Wiebe described in subsection 3.2 and 3.3. Next, the difference between the combustion parameters for hydrogen blends and only natural gas is computed for each H-NG blend at every load. This difference or delta in combustion parameters from the benchmark values of only natural gas performance at a fixed load is used to account for the changes in the in-cylinder combustion process due to hydrogen addition at that engine load.

In this study, the 75% load point is considered to be the nominal point for H-NG combustion as explained in the methodology subsection. Table 5.3 shows the 9 test points of different hydrogen blend percentages and engine loads used to understand the deviations in combustion parameters. The variations in load are represented by variations in normalized natural gas flow due to their linear relationship. For this purpose, the natural gas fuel mass injected per cylinder per cycle is normalized with respect to the nominal natural gas fuel mass measured at 75% engine load for 0H-NG fuel blend and 500 mg/Nm$^3$ of NOx. The delta in Seiliger and Wiebe combustion parameters are presented as a function of the normalized natural gas fuel ($m_{NG}^{norm}$) and volumetric hydrogen blend percentage ($H_V$) to study their trends and impact on the H-NG in-cylinder process over the engine load range.

Table 5.3: Tested hydrogen blend percentages and engine loads

| Engine Load [%] | H-NG Blends | NOx [mg/Nm$^3$] |
|---|---|---|
| 25 | 5, 10, 20 H-NG | 500 |
| 50 | 5, 10, 20H-NG | 500 |
| 75 | 5, 10, 20H-NG | 500 |

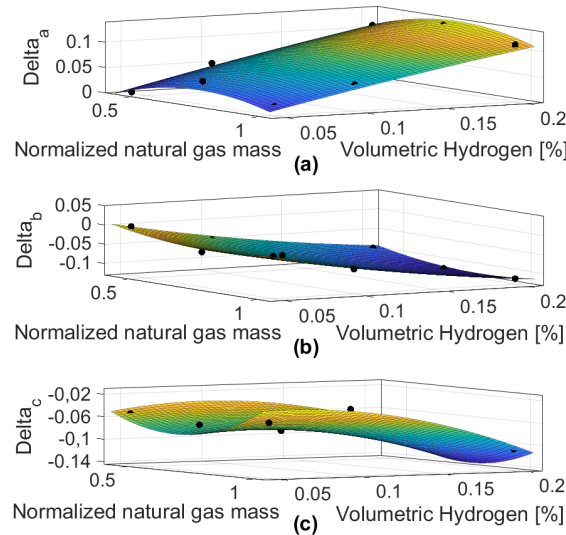## 5.2.1 Seiliger-based H-NG combustion modelling approach



Figure 5.6: Three-dimensional surface representation of the delta in Seiliger parameters 'a', 'b' and 'c' as a function of the normalized natural gas fuel mass and the volumetric hydrogen percentage.

Figure 5.6 shows the three-dimensional surface relationship for the deviations in Seilger parameters 'a', 'b' and 'c' as a function of the $m_{NG}^{norm}$ and $H_V$. It is evident from Figure 5.6 that the delta in Seilgier parameter 'a' increases at low normalized NG fuel mass or load, reaches a maximum value and then decreases at higher loads. The delta in Seiliger parameter 'a' goes on increasing with increasing hydrogen percentage at all loads. As explained in subsection 5.1.1, this increase in the value of 'a' with increasing hydrogen percentage can be

attributed to the increase in combustion heat release during stage 2-3 (at constant volume) due to the high combustion rate of hydrogen. Contrary to the deviation in 'a', delta in Seiliger parameter 'b' becomes negative with increasing hydrogen percentage. The delta in Seilgier parameter c becomes increasingly negative with increasing hydrogen percentage at all engine loads as seen from Figure 5.4, thus, reducing late combustion and combustion instability. In this manner, the deviations in Seilgier combustion parameters follow expected trends and can be easily understood for varying engine loads and hydrogen percentages.

The final value of a Seiliger parameter for an H-NG fuel blend and engine load is equal to the delta value added over the benchmark value of the parameter for only natural gas fuel. Using the computed values of Seiliger parameters, H-NG in-cylinder process is simulated for different engine loads and fixed 20 H-NG fuel blend. Table 5.4 lists the error percentages between simulated and measured values of performance parameters for varying engine loads. As seen from Table 5.4, Seiliger-based combustion characterization model is able to capture the H-NG combustion process over the engine load range with about 2% or lower deviations in estimations of work, exhaust pressure and temperature. Maximum in-cylinder pressure, temperature and combustion heat values are accurately simulated.

Table 5.4: Error percentages between the Seiliger combustion characterization simulation & measured values of performance parameters for 20H-NG fuel blend and 500 mg/Nm$^3$ of NOx at 75%, 50% and 25% engine load

| | $p_{max}$ | $T_{max}$ | Work | Net combustion heat | $p_6$ | $T_6$ |
|---|---|---|---|---|---|---|
| 20H-NG @ 500 mg/Nm$^3$ NOx, 75% load | 0 | -1.36e-04 | -0.68 | 9.92e-05 | -2.67 | -2.27 |
| 20H-NG @ 500 mg/Nm$^3$ NOx, 50% load | 0 | -1.65e-04 | -1.72 | 1.17e-04 | -2.11 | -2.1 |
| 20H-NG @ 500 mg/Nm$^3$ NOx, 25% load | 0 | -1.5e-05 | -1.92 | 1.13e-04 | -1.68 | -1.65 |

## 5.2.2 Double Wiebe function-based H-NG combustion modelling approach

Following the same above-described procedure, deviations in Wiebe combustion parameters are also found as a function of $m_{NG}^{norm}$ and $H_V$. Figure 5.7 shows the three-dimensional surface relationships for the deviations in Wiebe parameters due to hydrogen addition and engine loading. The Wiebe shape factor $m_1$ decreased with increasing load percentage. For a fixed engine load, the variations in primary combustion phase are small for different H-NG fuel blends as shown in subsection 5.1.2. Appendix 5 presents an additional discussion on the variations in $m_1$ and $m_2$ with load, hydrogen blend percentage and engine leaning. The delta of parameter $m_1$ should become increasingly positive with increasing hydrogen percentage as the heat release increases by a small margin. However, this trend is not followed for all hydrogen percentages and engine loads. This difficulty in identifying a clear trend and estimation of Wiebe shape factor was also reported by Rousseau et.al [35]. The delta in parameter $m_2$ increases in negative value with increasing hydrogen percentage at 75% engine load. Thus, the decrease in the overall value of $m_2$ with increasing hydrogen would represent a decrease in late combustion [46]. However, at some operating points of lower engine loads, the value of $m_2$ increased with increasing hydrogen percentage relative to the benchmark values of only natural gas performance. Based on the explanation given in subsection 5.1.2, this behaviour of $m_2$ is contrary to the expected trend of hydrogen addition decreasing $m_2$ and reducing late combustion. Thus, both Wiebe shape factors showcase difficulty in establishing clear tendencies at all loads and hydrogen percentages. Contrary to the shape factors, the delta in combustion duration $CD_1$ shows a clear decreasing trend for increasing hydrogen percentage at all engine loads as shown in Figure 5.7(c). This decreasing trend can be explained by the increasing combustion rate of the air-fuel mixture as the hydrogen percentage increases. Similar to $CD_1$, $CD_2$ also shows a general trend of decreasing total combustion duration with increasing hydrogen percentage. However, this expected trend was not found for all H-NG fuel blends at 75% engine load as seen from Figure 5.7(d) and also in subsection 5.1.2. This is due to the difficulty in accurately determining the exact end of combustion and the shape of end of combustion. Thus, the double Wiebe function-based combustion characterization process finds its limitation in identifying clear trends of shape parameters and $CD_2$ for all fuel blends and engine loads.

Using the derived values of Wiebe combustion parameters, H-NG in-cylinder process is simulated for different engine loads and 20 H-NG fuel blend. Table 5.5 lists the error percentages between simulated and measured values of performance parameters for varying engine loads using the Wiebe modelling approach. As seen from Table 5.5, double Wiebe function-based characterization model is able to capture the maximum pressure and temperature values within 2% deviation, while the exhaust pressure and temperature values deviate by a maximum of less than 3%. However, the errors in the estimation of work and net combustion heat are higher than those found for Seiliger in the previous subsection, with a maximum error of about 5.2%. As explained in subsection 4.2, the estimation of work and combustion heat is dependent on the fitted $RCO_{norm}$. The accuracy of this simulated $RCO_{norm}$ depends on the accurate estimation of Wiebe combustion parameters, which do not showcase clear tendencies with respect to load, hydrogen percentage and engine leaning. A small deviation in fitted $RCO_{norm}$ can produce errors in simulated work and heat.
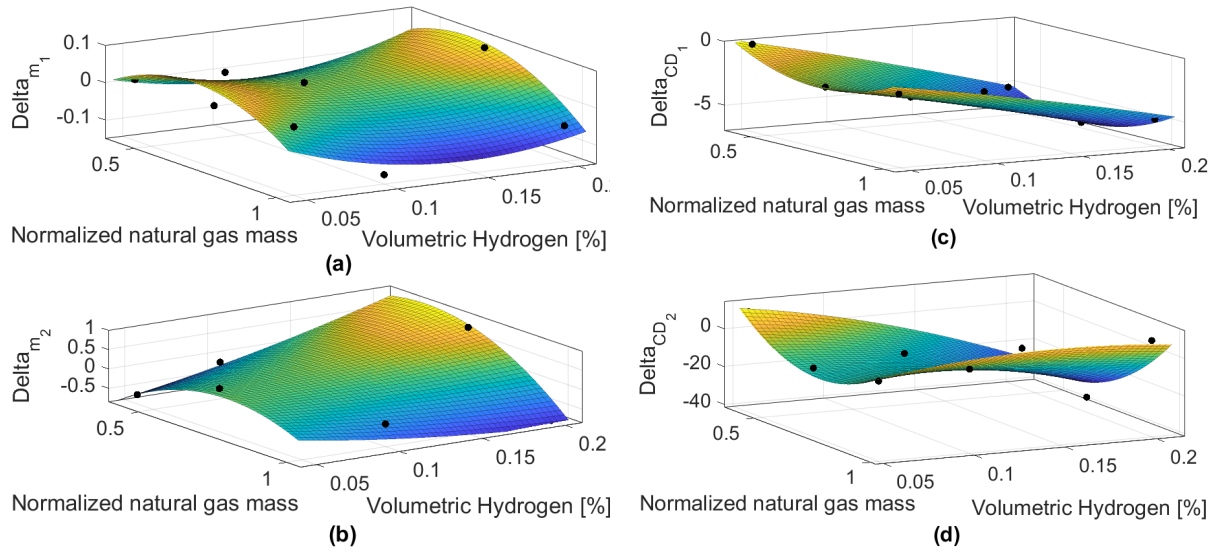
Figure 5.7: Three-dimensional surface representation of the delta in Wiebe combustion shape parameters 'm$_1$' (a), 'm$_2$' (b), CD$_1$ (c) and CD$_2$ (d) as a function of the normalized natural gas fuel mass and the volumetric hydrogen percentage

Table 5.5: Error percentages between the Wiebe combustion characterization simulation & measured values of performance parameters for for 20H-NG fuel blend and 500 mg/Nm$^3$ of NOx at 75%, 50% and 25% engine load

| | p$_{max}$ | T$_{max}$ | Work | Net combustion heat | p$_6$ | T$_6$ |
|---|---|---|---|---|---|---|
| **20H-NG @ 500 mg/Nm$^3$ NOx, 75% load** | -1.64 | 1.02 | -5.20 | -3.1 | -0.47 | -0.45 |
| **20H-NG @ 500 mg/Nm$^3$ NOx, 50% load** | -1.66 | 0.51 | -5.22 | -5.25 | -2.94 | -2.93 |
| **20H-NG @ 500 mg/Nm$^3$ NOx, 25% load** | -1.30 | 0.64 | -4.26 | -2.33 | -0.05 | -0.03 |

Based on the above-described characterization of H-NG combustion, Seiliger combustion parameters showcase clear trends and good ability in capturing the H-NG combustion process variations for different H-NG fuel blends, loads and engine leaning. By identifying clear trends in variations of combustion parameters, parametric equations can be derived in future as a function of normalized natural gas fuel (load), volumetric hydrogen blend percentage and air-excess ratio to capture the H-NG combustion process and engine performance under varying test conditions that could not be tested experimentally. Furthermore, the derived parametric equations for Seiliger and Wiebe combustion models can be combined with mean value engine models to perform system integration, load variations and engine control studies, thus, extending the application of the modelling approaches and research presented in this paper.

# 6    CONCLUSIONS AND RECOMMENDATIONS

This paper investigated and compared the capabilities of Seiliger and Wiebe-based modelling approaches to characterize and capture the H-NG combustion process in a marine lean-burn SI engine. The conclusions drawn from this study are as follows:

- The study presented a detailed methodology to develop 0-D Seiliger and double Wiebe function-based H-NG combustion characterization models based on engine measurements to study and capture the combustion process for different H-NG fuel blends, engine loads and engine leaning. To simulate the heat release process of H-NG fuel blends based on engine measurements, a single-zone, 0-D, thermodynamic heat release rate (HRR) model was developed. The developed HRR model accounted for the impact of high amount of trapped residual gas found in the zero valve overlap test engine. The model also accounted for the increase in trapped mixture temperature due to the mixing of inducted mass with the hot residual combustion gases trapped from the previous cycle. The HRR model formed the first step towards the characterization of H-NG combustion using the Seiliger and double Wiebe function-based modelling approaches.

- The study found that Seiliger parameters 'a', 'b' and 'c' represent different physical phenomenon in the H-NG combustion process. Seiliger parameter 'a' can be directly related to the increase in combustion rate with increasing hydrogen addition. Seiliger parameter 'b' signified a measure of combustion stability while Seiliger parameter 'c' represented late combustion present in lean-burn combustion.

22

- A double-Wiebe function with combustion parameters 'm$_1$', 'm$_2$', 'CD$_1$' and 'CD$_2$' was presented to characterize the H-NG combustion process. In the Wiebe characterization process, the second Wiebe function helped capture the changes in late burn phase found in lean-burn NG and H-NG combustion.
- This study showed that the characterization of H-NG combustion using the Seiliger modelling approach can be used to capture the H-NG in-cylinder combustion process with high accuracy. Similarly, H-NG combustion can be simulated by using the Wiebe modelling approach with accurate estimation of the in-cylinder pressures and temperatures, however, it produced higher deviations in the estimation of work output and combustion heat for different H-NG fuel blends, engine leaning and loads. The Wiebe-based approach produced a maximum error of about 5.2% for both work output and combustion heat, while Seiliger error was less than 2% for both these variables.
- The better ability of Seiliger than Wiebe to capture the variations in H-NG combustion process for different fuel blends, engine leaning and loads could be attributed to the following factors:
  - Limitation of double Wiebe function in identifying clear trends of the Wiebe shape parameters and the combustion duration of the second Wiebe function (CD$_2$) for all fuel blends, engine leaning and loads.
  - Difficulty in the accurate fitting of normalized RCO.
- The H-NG combustion characterization process showed that maximum in-cylinder pressures and temperatures decreased with engine leaning, while hydrogen addition at the same NOx emission increased the maximum in-cylinder pressure values. The characterization process also showed that as the air-intake is controlled, the engine produces almost similar values of maximum in-cylinder temperatures to produce the same amount of NOx emissions. Therefore, the combustion due to hydrogen addition could be controlled by governing the air-intake to control the maximum in-cylinder temperatures to produce NOx emissions within IMO TIER-III NOx emission limits.

The following recommendations are presented for future work:

- The Seiliger and Wiebe modelling approaches presented in this paper can be combined with a mean value open cycle model to produce combustion effects in sufficient detail while capturing total engine performance dynamics. Such Seiliger and Wiebe-based MVEMs can be employed to study controls, load variations, system integration, voyage simulations and even smart maintenance strategies for ships.
- The authors recommend the Seiliger based approach due to its ability to accurately capture the variations in the combustion process at all the crucial points with low computation effort due to the discretized in-cylinder process.
- The presented methodology and modelling approaches could be applied to other alternative fuels and automotive engines.
- Parametric equations can be derived to compute Seiliger and Wiebe combustion parameters as a function of normalized natural gas fuel (load) and hydrogen percentage using regression fitting. This will help develop generic and validated parametric equations that can be used to capture the H-NG combustion process and engine performance under varying test conditions.

## ACKNOWLEDGEMENTS

## APPENDIX 1: PARAMETERS SIMULATED BY THE SEILGIER AND WIEBE MODELLING APPROACH

In this paper, $p_{max}$, $T_{max}$, work, net combustion heat, $p_6$ and $T_6$ modelling parameters chosen for the purpose of comparison between the two capabilities of two modelling approaches as these are vital parameters for simulation studies on system integration, controls and load variations. Other parameters such as pressure at CA10, CA50 and CA90 along with the maximum rate of pressure rise and their corresponding crank angles can be vital parameters for combustion characterization. However, it is vital to note that the choice of the modelling approach is dictated by the modelling objective, which is followed by three other factors, i.e., the

level of detail, modelling accuracy and computational effort. The Seiliger modelling approach provides sufficient details of the in-cylinder and combustion process that can be accurately captured with variations in operating parameters such as load, leaning and H-NG fuel blends along with low computational effort. This makes the Seiliger modelling approach in combination with Mean Value Engine Models (MVEMs) ideal for studying system integration, voyage simulations, engine control, load variations and smart maintenance of ships. At the same time, it is vital to understand the inability of the Seiliger modelling approach in capturing crank angle resolved information without the HRR model as shown in Table A1.1. As seen from Table A1.1, $p_{max}$, $T_{max}$, work, net combustion heat, $p_6$ and $T_6$ are the common parameters that are directly available from both the modelling approaches. Therefore, these parameters can be used to compare the capabilities of the Seiliger and Wiebe modelling approach in capturing the H-NG in-cylinder and combustion process.

Table A1.1: Parameters simulated by the Seiliger and Wiebe modelling approach. A: Available, NA: Not Available, AwHRR: Available with HRR model

| Parameter | Seiliger | Wiebe |
|---|---|---|
| $p_{max}$ | A | A |
| $T_{max}$ | A | A |
| Work | A | A |
| Heat | A | A |
| $p_6$ | A | A |
| $T_6$ | A | A |
| CA10 | NA | A |
| $P_{@CA10}$ | NA | A |
| CA50 | NA | A |
| $P_{@CA50}$ | AwHRR | A |
| CA90 | NA | A |
| $P_{@CA90}$ | AwHRR | A |
| CA(C) | NA | A |
| $P_{@CA(C)}$ | AwHRR | A |
| $CA(dp/dt_{max})$ | NA | A |
| $dp/dt_{max}$ | NA | A |
| $T_{@CA10}$ | NA | A |
| $T_{@CA50}$ | AwHRR | A |
| $T_{@CA90}$ | AwHRR | A |
| $T_{@CAC}$ | AwHRR | A |

Crank angle based information such as CA10, CA50 and CA90 can be determined using the double Wiebe function. Additionally, the in-cylinder pressure values at CA10, CA50, CA90 and the maximum rate of pressure rise can be determined using the Wiebe modelling approach. On the other hand, CA10, CA50 and CA 90 cannot be determined using Seiliger, since Seiliger is a 5-stage discretized in-cylinder model and not a crank angle based model. Table A1.2 provides the error percentages between the double Wiebe function-based combustion characterization simulation & measured values of performance parameters for 20H-NG fuel blend and 500 mg/Nm$^3$ NOx value at 75% engine load.

Table A1.2: Error percentages between the Wiebe combustion characterization simulation & measured values of crank angle resolved parameters for 20H-NG fuel blend and 500 mg/Nm$^3$ NOx values at 75% engine load.

| | CA10 | $P_{@CA10}$ | CA50 | $P_{@CA50}$ | CA90 | $P_{@CA90}$ | $CA(dp/dt_{max})$ | $dp/dt_{max}$ | $T_{@CA10}$ | $T_{@CA50}$ | $T_{@CA90}$ |
|---|---|---|---|---|---|---|---|---|---|---|---|
| Measured | 179.9 | 54.57 | 195.9 | 67.5 | 242 | 18.32 | 184.9 | 1.254 | 879.6 | 1346 | 1235 |
| Wiebe | 180.7 | 57.46 | 195.1 | 66.54 | 237.8 | 20.23 | 175 | 1.272 | 926.8 | 1303 | 1244 |
| Error % | 0.444 | 5.29 | -0.408 | -1.42 | -1.74 | 10.45 | 5.354 | 1.435 | 5.36 | -3.19 | 0.7234 |

As shown in Table A1.2, the double Wiebe function can be used to compute crank angle resolved information with a maximum error of 10.45 % in the estimation of pressure at CA90. The error in estimation can be attributed to the difficulty in accurately capturing the end of combustion and also the difficulty in the accurate fitting of RCO as mentioned section 5.1.2 and section 4.2. Although, by definition, Seiliger cannot provide

values of crank angles corresponding to CA10, CA50 and CA90, error percentages can be computed for pressures and temperatures corresponding to CA10, CA50 and CA90 using Seiliger assuming the corresponding crank angle positions are known from the HRR model as shown in Table A1.1. Table A1.3 provides these error percentages.

Table A1.3: Error percentages between the Seiliger combustion characterization simulation & measured values of crank angle resolved parameters for 20H-NG fuel blend and 500 mg/Nm$^3$ NOx values at 75% engine load. Note: Corresponding crank angles are obtained from the HRR model

| | CA $_{(c)}$ | p@CA10 | P@CA50 | P@CA90 | p@CA(c) | dp/dt$_{max}$ | T$_{@CA10}$ | T$_{@CA\,50}$ | T$_{@CA90}$ | T$_{@CA(c)}$ |
|---|---|---|---|---|---|---|---|---|---|---|
| Measured | 217.4 | 54.57 | 67.5 | 18.32 | 39.3 | 1.254 | 879.6 | 1346 | 1235 | 1430 |
| Seiliger | NA | 67.84 | 67.84 | 18.12 | 40.24 | NA | 740.1 | 1359 | 1221 | 1467 |
| Error % | NA | 24.31 | 0.5 | -1.09 | 0.865 | NA | -15.85 | 0.96 | -1.13 | 2.58 |

Table A1.3 shows that Seiliger produces large errors for pressure and temperature estimation at CA10 as the Seiliger process switches from stage 2 to 3 when CA10 occurs. On the other hand, Seiliger simulates pressures and temperatures at CA50 and CA90 with good accuracy as these points lie close to Seiliger stages. The Seiliger modelling approach is not capable of capturing the maximum rate of pressure rise as this value is infinity for the Seiliger modelling approach by definition. In the Seiliger process, the end of combustion corresponds to the end of the isothermal combustion stage, which is depicted by the Seiliger parameter 'c'. Table A1.3 also provides the error in estimation of pressure and temperature by Seiliger compared to the measured values at point 'c'.

To summarize the above discussion, although the Wiebe modelling approach provides additional crank angle resolved information of the combustion process, the Seiliger modelling approach is capable of providing sufficient details of the H-NG in-cylinder and combustion process while accurately capturing the variations in the H-NG in-cylinder and combustion process for varying operating parameters with low computational effort. The variations in the combustion process are not well captured by the Wiebe modelling approach as explained in section 5.1.2 and 5.2.2 of the paper. Thus, both the Seiliger and Wiebe modelling approaches have their own advantages and limitations, which can dictate the choice of the modelling approach.

## APPENDIX 2: DERIVATION OF TRAPPED AIR-FRACTION

The derivation of trapped air mass fraction as a function of the residual gas mass fraction, air-excess ratio (λ) and the stoichiometric air-to-fuel ratio is as follows [48]:

The trapped air fraction ($x_{air,t}$) can be written as a function of the trapped residual gas fraction ($x_{rg,t}$) and trapped fuel fraction ($x_{f,t}$),

$$x_{air,t} = (1 - x_{rg,t}) - x_{f,t}$$ 
A2.1

where, $x_{air,t} = \dfrac{m_{air,t}}{m_t}$ ; $x_{rg,t} = \dfrac{m_{rg,t}}{m_t}$ ; $x_{f,t} = \dfrac{m_{f,t}}{m_t}$ $m_t$: trapped mass

Equation A1.1 can be written in the following manner,

$$\frac{m_{air,t}}{m_t} = (1 - \frac{m_{sg,t}}{m_t}) - \frac{m_{f,t}}{m_t}$$
A2.2

Multiplying both sides of equation A2.2 by the ratio of trapped air mass and trapped fuel mass,

$$\frac{m_{air,t}}{m_t} \cdot \frac{m_{air,t}}{m_{f,t}} = (1 - \frac{m_{rg,t}}{m_t}) \cdot \frac{m_{air,t}}{m_{f,t}} - \frac{m_{f,t}}{m_t} \cdot \frac{m_{air,t}}{m_{f,t}}$$
A2.3

Equation A2.3 can be simplified by writing the term as a function of stoichiometric air-to-fuel ratio and air-excess ratio:

$$\frac{m_{air,t}}{m_{f,t}} = \frac{m_{air,min}}{m_{f,t}} \cdot \frac{m_{air,t}}{m_{air,min}} = \sigma \cdot \lambda$$
A2.4

Substituting equation A2.4 into equation A2.3, and using the mass fraction definitions:

$$x_{air,t} \cdot \sigma \cdot \lambda = (1 - x_{rg,t}) \cdot \sigma \cdot \lambda - x_{air,t}$$
A2.5

Rearranging equation A2.5 gives,

$$x_{air,t} = \frac{(1 - x_{rg,t}) \cdot \sigma \cdot \lambda}{\sigma \cdot \lambda + 1}$$ A2.6

# APPENDIX 3: DERIVATION OF TRAPPED MIXTURE TEMPERATURE FOR SI NG ENGINE WITH ZERO VALVE OVERLAP

In a conventional 4-stroke engine with a positive valve overlap, the trapped mass ($m_t$) is represented by equation A3.1.

$$m_t = m_{ind} + m_{rg,t} + m_{ret}$$ A3.1

where, $m_{ind}$: air-fuel mass drawn into the cylinder during the induction stroke; $m_{rg,t}$: residual mass of combustion gas trapped from the previous cycle; $m_{ret}$: part of scavenging mass retained after either the inlet or outlet valve closing.

In a natural gas engine with zero valve overlap, there is no scavenging and, therefore, retained mass in equation A3.1 is zero. Thus, the total trapped mass becomes

$$m_t = m_{ind} + m_{rg,t}$$ A3.2

Each mass term in equation A3.2 is solved individually to calculate the trapped mixture temperature since the trapped temperature has a combined effect of the increased induction temperature and temperature due to mixing with the hot residual combustion gases trapped from the previous cycle. Starting with the total trapped and applying the ideal gas equation, we get:

$$m_t = \frac{p_t \cdot V_t}{R \cdot T_t} = \frac{p_t \cdot V_{IC}}{R \cdot T_t}$$ A3.3

where, $V_t$: trapped volume and is equal to the cylinder volume at the moment of inlet valve closing. The trapped volume is estimated from crank angle measurements [47].

Similarly, the induction mass is written as,

$$m_{ind} = \frac{p_t \cdot V_{ind}}{R \cdot T_{ind}} = \frac{p_t \cdot (V_{IC} - V_{IO})}{R \cdot T_{ind}}$$ A3.4

where, $p_t$: trapped pressure is obtained from measurements; R: gas constant; $V_{ind}$: induction volume between inlet valve opening and closing. In this engine with zero valve overlap, the inlet valve opens after the exhaust valve closes, thus, starting the induction stroke. This induction stroke ends with the closing of the inlet valve as shown in Table 2.2. The cylinder volumes at the time of inlet valve closing and opening can be determined from geometrical formulations using the crank angle measurements.

In equation A3.4 the induction temperature ($T_{ind}$) is estimated in the following manner. During the induction stroke as the mass enters the cylinder; its temperature will be higher than the temperature at inlet manifold due to heat-pick-up from the inlet duct walls [67]. Therefore, the induction temperature is determined from the measured manifold temperature ($T_{man}$) by using equation A3.5 [67],

$$T_{ind} = \varepsilon_{inl} \cdot T_{inl} + (1 - \varepsilon_{inl}) \cdot T_{man}$$ A3.5

where, $\varepsilon_{inl}$: heat exchange effectiveness = 0.05; $T_{in}$: inlet manifold duct wall temperature = 400 K [67].

After determining the trapped and induction mass, the residual mass in equation A3.2 is derived. In the test engine with zero valve overlap, the exhaust blowdown process (exhaust stroke) begins with the opening of the exhaust valve and then ends with the closing of the exhaust valve. During the blowdown process, the mass in the cylinder expands to pressure and temperature equivalent to the pressure and temperature in the exhaust receiver manifold [67]. Thus, after the exhaust stroke or blowdown process, the pressure and the temperature of the mass still remaining inside the cylinder is equal to the blowdown pressure ($P_{bld}$) and blowdown temperature ($T_{bld}$). In the experiments performed for this study, the pressure in the exhaust receiver was measured, which is equivalent to the blowdown pressure. Assuming a polytropic blowdown process, the blowdown temperature can be computed from the measured blowdown pressure and the pressure at the moment of exhaust valve opening ($p_{EO}$).

$$T_{bld} = (\frac{p_{bld}}{p_{EO}})^{(\frac{n_e-1}{n_e})} \cdot T_{EO} \qquad \text{A3.6}$$

where, $p_{EO}$ is the pressure at the moment of exhaust valve opening obtained from in-cylinder pressure measurements; $n_e$: polytropic exponent; $T_{EO}$: in-cylinder temperature at the moment of exhaust valve opening. It is calculated by applying the ideal gas equation at the moment of exhaust valve opening. At this point, the mass in the cylinder ($m_{EO}$) is equal to the trapped mass, since the in-cylinder mas is assumed to be constant without any crevice mass losses.

$$T_{EO} = \frac{p_{EO} \cdot V_{EO}}{R \cdot m_{EO}} \qquad \text{A3.7}$$

After calculating the blowdown temperature, the trapped residual mass of combustion gas left after the blowdown process or at the point of exhaust valve closing is given by,

$$m_{rg,t} = \frac{p_{bld} \cdot V_{EC}}{R \cdot T_{bld}} \qquad \text{A3.8}$$

where $V_{EC}$ is the cylinder volume at the time of exhaust valve closing and is determined from geometrical formulations using the crank angle measurements.

To calculate the trapped temperature, equations A4.3, A4.4 and A4.8 are substituted in equation A3.2.

$$\frac{p_t \cdot V_{IC}}{R \cdot T_t} = \frac{p_t \cdot (V_{IC} - V_{IO})}{R \cdot T_{ind}} + \frac{p_{bld} \cdot V_{EC}}{R \cdot T_{bld}} \qquad \text{A3.9}$$

Although the gas constant is a function of the mixture composition, it changes minutely for trapped, induction and residual mass, therefore, it can be assumed constant. By simply rearranging the equation A3.9, trapped mixture temperature is determined as a combination of the heat pick-up during induction and the high blowdown temperature of the residual combustion gas.

$$\frac{1}{T_t} = \frac{(V_{IC} - V_{IO})}{V_{IC} \cdot T_{ind}} + \frac{(V_{EC} \cdot P_{bld})}{V_{IC} \cdot P_t \cdot T_{bld}} \qquad \text{A3.10}$$

## APPENDIX 4: SEILIGER PROCESS MODEL EQUATIONS

Table A4.1: Analytical correlations in the five-stage Seiliger process [37]

| Seiliger Stage | Volume Ratio | Pressure Ratio | Temperature Ratio | Seiliger Parameters |
|---|---|---|---|---|
| 1 – 2 | $\frac{V_1}{V_2} = r_c$ | $\frac{p_2}{p_1} = r_c^{n_c}$ | $\frac{T_2}{T_1} = r_c^{n_c-1}$ | $r_c$, $n_c$ |
| 2 – 3 | $\frac{V_3}{V_2} = 1$ | $\frac{p_3}{p_2} = a$ | $\frac{T_3}{T_2} = a$ | $a$ |
| 3 – 4 | $\frac{V_4}{V_3} = b$ | $\frac{p_4}{p_3} = 1$ | $\frac{T_4}{T_3} = b$ | $b$ |
| 4 – 5 | $\frac{V_5}{V_4} = c$ | $\frac{p_4}{p_5} = c$ | $\frac{T_5}{T_4} = 1$ | $c$ |
| 5 – 6 | $\frac{V_6}{V_5} = r_e$ | $\frac{p_5}{p_6} = r_e^{n_e}$ | $\frac{T_5}{T_6} = r_e^{n_e-1}$ | $r_e$, $n_e$ |

| Seiliger Stage | Work per unit mass [kJ/kg] | Heat per unit mass [kJ/kg] |
|---|---|---|
| 1 – 2 | $w_{12} = -\dfrac{1}{n_c - 1} \cdot R \cdot (T_2 - T_1)$ | $q_{12} = -[\dfrac{1}{n_c - 1} - \dfrac{1}{\gamma - 1}] \cdot R \cdot (T_2 - T_1)$ |
| 2 – 3 | $w_{23} = 0$ | $q_{23} = c_v \cdot (T_3 - T_2)$ |
| 3 – 4 | $w_{34} = R \cdot (T_3 - T_4)$ | $q_{34} = c_v \cdot (T_4 - T_3)$ |
| 4 – 5 | $w_{45} = R \cdot T_4 \cdot \ln(c)$ | $q_{45} = R \cdot T_4 \cdot \ln(c)$ |
| 5 – 6 | $w_{56} = \dfrac{1}{n_e - 1} \cdot R \cdot (T_5 - T_6)$ | $q_{56} = -[\dfrac{1}{\gamma - 1} - \dfrac{1}{n_e - 1}] \cdot R \cdot (T_5 - T_6)$ |

## APPENDIX 5: VARIATIONS IN WIEBE SHAPE PARAMETERS

Figure A5.1(a) and Figure A5.1(b) show the non-dimensional combustion or heat release rate for different values of $m_1$ and $m_2$ while the remaining Wiebe parameters are kept constant at values found for 10H-NG fuel blend and 500 mg/Nm$^3$ of NOx at 75% engine load. This can help understand the expected variations in heat release as $m_1$ and $m_2$ change. In this analysis, each case of varying load, hydrogen percentage and engine leaning has been discussed separately.

**Case 1: Load**

In [46], Ding used the double Wiebe function for diesel combustion with values of $m_1$ varying from 0.05 to 0.5. For this range of $m_1$, the non-dimensional combustion rate increased with decreasing $m_1$. For the H-NG combustion studied in this paper, the value of $m_1$ varied from 2.5 to 3.5. As seen from Figure A5.1(a), the non-dimensional combustion rate during the primary phase of combustion increases as $m_1$ varies from 2.5 to 3.5. However, variations in $m_2$ impact the heat release during the primary phase of combustion. An increase in value of $m_2$ means more heat is released in the late combustion phase and less is released during the primary combustion phase and vice versa. This impact of $m_2$ on the primary phase of combustion is evident in Figure A5.1(b) and helps understand the heat release during load variations.

Based on the HRR model analysis, the decrease in engine load reduced the heat released during late combustion. The decrease in late combustion reduced the value of $m_2$ for lower loads, which increased the non-dimensional heat released during the primary phase of combustion as seen from Figure 5.1(b). The increased normalized heat release in the primary phase of combustion was accompanied by an increased $m_1$ for lower loads. Therefore, $m_1$ decreased with increasing load as stated in section 5.2.2. However, this does not mean that the absolute heat release during the primary phase of combustion is higher for lower loads. The absolute value is a multiple of the non-dimensional heat release and the fuel mass, divided by combustion time [46]. Since the fuel mass is low at lower loads compared to the mass at higher loads, the absolute heat release is higher for higher loads even though the non-dimensional heat release is lower due to a lower value of $m_1$ and $m_2$.
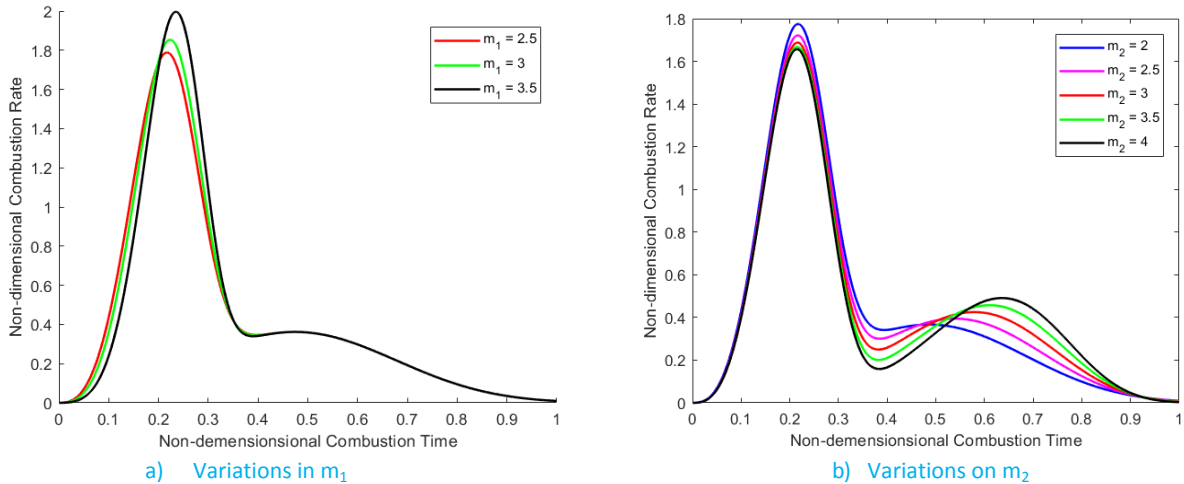


a) Variations in $m_1$  b) Variations on $m_2$

Figure A5.1: Non-dimensional combustion rate for increasing value of $m_1$(a) and $m_2$(b) while other Wiebe combustion parameters are fixed at value found for 10H-NG fuel blend, 500 mg/Nm$^3$ NOx at 75% engine load

**Case 2: Hydrogen percentage**

In this case, $m_2$ decreases with increasing hydrogen percentage as hydrogen reduces late combustion. A lower value of $m_2$ contributes to the heat release in the primary combustion phase as shown in Figure A5.1(b). More non-dimensional heat is released in the primary combustion phase with hydrogen addition and an increased value of $m_1$ as seen in Figure A5.1(a). However, this increment in $m_1$ was not found at all loads for increasing hydrogen percentages as shown in Figure 5.7(b) and explained in section 5.2.2.

**Case 3: Engine leaning**

During engine leaning to lower values of NOx, more heat is released during the late combustion phase, which is depicted by increasing $m_2$ as seen in Figure 5.4(a). Higher the value of $m_2$, higher the non-dimensional heat release in the last combustion phase and lower the heat released in the primary combustion phase, which is evident from Figure A5.1(b). Thus, the increasing value of $m_2$ indicates deterioration of the combustion process. Additionally, engine leaning was accompanied by a decreased value of $m_1$ as seen in Table 4.6.

## REFERENCES

[1]     R. K. Mehra, H. Duan, R. Juknelevičius, F. Ma, and J. Li, "Progress in hydrogen enriched compressed natural gas (HCNG) internal combustion engines - A comprehensive review," *Renew. Sustain. Energy Rev.*, vol. 80, no. December, pp. 1458–1498, 2017.

[2]     D. P., R. Kumar P, and V. Kumar D., "Lean combustion technology for internal combustion engines: A review," *Sci. Technol.*, vol. 2, no. 1, pp. 47–50, 2012.

[3]     D. Dunn-Rankin, *Lean Combustion: Technology and Control*. Elsevier, 2008.

[4]     L. Xiang, E. Song, and Y. Ding, "A two-zone combustion model for knocking prediction of marine natural gas SI engines," *Energies*, vol. 11, no. 3, p. 561, 2018.

[5]     K. Packham, "Lean-burn engine technology increases efficiency , reduces NOx emissions," White paper, Cummins Power Generation, 2007.

[6]     H. Sapra, Y. Linden, W. van Sluijs, M. Godjevac, and K. Visser, "Experimental investigations of performance variations in marine hydrogen-natural gas engines," in *Cimac Congress 2019*, 2019, pp. 1–17.

[7]     CIMAC WG17 "Gas Engines," "Transient response behaviour of gas engines," *Position Pap. Int. Concil Combust. Engines*, pp. 1–7, 2011.

[8]     H. Sapra, Y. Linden, W. van Sluijs, M. Godjevac, and K. Visser, "Experimental investigations of hydrogen-natural gas engines for maritime applications," in *ASME 2018 Internal Combustion Fall Technical Conference ICEF2018*, 2018.

[9]     M. Godjevac and M. Drijver, "Power configurations of an inland pusher," in *ICMT 2014*, 2014, no. July, pp. 1–10.

[10]    F. Ma and Y. Wang, "Study on the extension of lean operation limit through hydrogen enrichment in a natural gas spark-ignition engine," *Int. J. Hydrogen Energy*, vol. 33, no. 4, pp. 1416–1424, 2008.

[11]    Y. Ra and R. D. Reitz, "A combustion model for IC engine combustion simulations with multi-component fuels," *Combust. Flame*, vol. 158, no. 1, pp. 69–90, 2011.

[12]    E. Hendricks, "Engine Modelling for Control Applications: A Critical Survey," *Meccanica*, vol. 32, no. 5, pp. 387–396, 1997.

[13]    S. I. Raptotasios, N. F. Sakellaridis, R. G. Papagiannakis, and D. T. Hountalas, "Application of a multi-zone combustion model to investigate the NOx reduction potential of two-stroke marine diesel engines using EGR," *Appl. Energy*, vol. 157, pp. 814–823, 2015.

[14]    G. Benvenuto and U. Campora, "Dynamic simulation of a high- performance sequentially turbocharged marine diesel engine," *J. Eng. Marit. Environ.*, vol. 3, no. 3, pp. 115–125, 2011.

[15]    R. Schulz, Y. M. Wright, and K. Boulouchos, "Progress in computational fluid dynamics (CFD) Applications for large diesel engine development," in *CIMAC Congress 2004*, 2004.

[16]    M. Baratta, D. Misul, L. Viglione, and J. Xu, "Combustion chamber design for a high-performance natural gas engine: CFD modeling and experimental investigation," *Energy Convers. Manag.*, vol. 192, pp. 221–231, Jul. 2019.

[17]    R. D. Geertsma, R. R. Negenborn, K. Visser, M. A. Loonstijn, and J. J. Hopman, "Pitch control for ships with diesel mechanical and hybrid propulsion: Modelling, validation and performance quantification," *Appl. Energy*, vol. 206, no. April, pp. 1609–1631, 2017.

[18]    M. S. Cellek and A. Pınarbaşı, "Investigations on performance and emission characteristics of an

industrial low swirl burner while burning natural gas, methane, hydrogen-enriched natural gas and hydrogen as fuels," *Int. J. Hydrogen Energy*, vol. 43, no. 2, pp. 1194–1207, Jan. 2018.

[19]  J. Zareei, A. Rohani, and W. M. F. Wan Mahmood, "Simulation of a hydrogen/natural gas engine and modelling of engine operating parameters," *Int. J. Hydrogen Energy*, vol. 43, no. 25, pp. 11639–11651, Jun. 2018.

[20]  X. Ling, F. Wu, and D. Yao, "A reduced combustion kinetic model for the methanol-gasoline blended fuels on SI engines," *Sci. China Technol. Sci.*, vol. 59, no. 1, pp. 81–92, Jan. 2016.

[21]  A. Kakoee and A. Gharehghani, "Comparative study of hydrogen addition effects on the natural-gas/diesel and natural-gas/dimethyl-ether reactivity controlled compression ignition mode of operation," *Energy Convers. Manag.*, vol. 196, pp. 92–104, Sep. 2019.

[22]  İ. Altın and A. Bilgin, "Quasi-dimensional modeling of a fast-burn combustion dual-plug spark-ignition engine with complex combustion chamber geometries," *Appl. Therm. Eng.*, vol. 87, pp. 678–687, Aug. 2015.

[23]  X. Duan, Y. Liu, J. Liu, M.-C. Lai, M. Jansons, G. Guo, S. Zhang, and Q. Tang, "Experimental and numerical investigation of the effects of low-pressure, high-pressure and internal EGR configurations on the performance, combustion and emission characteristics in a hydrogen-enriched heavy-duty lean-burn natural gas SI engine," *Energy Convers. Manag.*, vol. 195, pp. 1319–1333, Sep. 2019.

[24]  C. D. Rakopoulos, M. A. Scott, D. C. Kyritsis, and E. G. Giakoumis, "Availability analysis of hydrogen/natural gas blends combustion in internal combustion engines," *Energy*, vol. 33, no. 2, pp. 248–255, Feb. 2008.

[25]  L. Xiang, G. Theotokatos, and Y. Ding, "Investigation on gaseous fuels interchangeability with an extended zero-dimensional engine model," *Energy Convers. Manag.*, vol. 183, pp. 500–514, Mar. 2019.

[26]  C. D. Rakopoulos and C. N. Michos, "Development and validation of a multi-zone combustion model for performance and nitric oxide formation in syngas fueled spark ignition engine," *Energy Convers. Manag.*, vol. 49, no. 10, pp. 2924–2938, Oct. 2008.

[27]  M. Yıldız and B. Albayrak Çeper, "Zero-dimensional single zone engine modeling of an SI engine fuelled with methane and methane-hydrogen blend using single and double Wiebe Function: A comparative study," *Int. J. Hydrogen Energy*, vol. 42, no. 40, pp. 25756–25765, Oct. 2017.

[28]  Y. Tang, J. Zhang, H. Gan, B. Jia, and Y. Xia, "Development of a real-time two-stroke marine diesel engine model with in-cylinder pressure prediction capability," *Appl. Energy*, vol. 194, pp. 55–70, 2017.

[29]  J. I. Ghojel, "Review of the development and applications of the Wiebe function: a tribute to the contribution of Ivan Wiebe to engine research."

[30]  G. Abbaszadehmosayebi and L. Ganippa, "Determination of specific heat ratio and error analysis for engine heat release calculations," *Appl. Energy*, vol. 122, pp. 143–150, Jun. 2014.

[31]  J. B. Heywood, *Internal combustion engine fundamentals*. New York : McGraw-Hill, 1988.

[32]  J. Liu and C. E. Dumitrescu, "Single and double Wiebe function combustion model for a heavy-duty diesel engine retrofitted to natural-gas spark-ignition," *Appl. Energy*, vol. 248, pp. 95–103, Aug. 2019.

[33]  G. J. Amador Diaz, J. P. Gómez Montoya, L. A. Corredor Martinez, D. B. Olsen, and A. Salazar Navarro, "Influence of engine operating conditions on combustion parameters in a spark ignited internal combustion engine fueled with blends of methane and hydrogen," *Energy Convers. Manag.*, vol. 181, pp. 414–424, Feb. 2019.

[34]  J. L. E. Carrera, J. M. A. Riesco, S. M. Martinez, F. A. C. Sanchez, and A. M. Gallegos, "Numerical study on the combustion process of a biogas spark ignition engine," *Thermal Science*, vol. 17, no. 1. pp. 241–254, 2013.

[35]  S. Rousseau, B. Lemoult, and M. Tazerout, "Combustion characterization of natural gas in a lean burn spark-ignition engine," vol. 213, no. x, pp. 481–490, 1999.

[36]  S.-S. Hou, "Heat transfer effects on the performance of an air standard Dual cycle," *Energy Convers. Manag.*, vol. 45, no. 18–19, pp. 3003–3015, Nov. 2004.

[37]  D. Stapersma, *Diesel engines : A fundamental approach to performance analysis, turbocharging, combustion, emissions and heat transfer including thermodynamical principles. Vol. 1: Performance analysis.* Delft: TU Delft, 2010.

[38]  Y. Ding, C. Sui, and J. Li, "An experimental investigation into combustion fitting in a direct injection marine diesel engine," *Appl. Sci.*, vol. 8, no. 12, p. 2489, 2018.

[39]  C. Sui, E. Song, D. Stapersma, and Y. Ding, "Mean value modelling of diesel engine combustion based on parameterized finite stage cylinder process," *Ocean Eng.*, vol. 136, pp. 218–232, May 2017.

[40]  I. Georgescu, D. Stapersma, and B. Mestemaker, "Dynamic behaviour of gas and dual-fuel engines :

Using models and simulations to aid system integration," *Int. Counc. Combust. Engines Congr.*, 2016.

[41]	H. Sapra, M. Godjevac, K. Visser, D. Stapersma, and C. Dijkstra, "Experimental and simulation-based investigations of marine diesel engine performance against static back pressure," *Appl. Energy*, vol. 204, pp. 78–92, 2017.

[42]	P. Skogtjarn, "Modelling of the exhaust gas temperature for diesel engines," Linkopings University, 2002.

[43]	S. Schlesinger, R. E. Crosbie, R. E. Gagn, G. S. Innis, C. Lalwani, J. Loch, R. J. Sylvester, R. D. Wright, N. Kheir, and D. Bartos, "Terminology for model credibility."

[44]	A. Vrijdag, D. Stapersma, and T. Van Terwisga, "Systematic modelling, verification, calibration and validation of a ship propulsion simulation model," *J. Mar. Eng. Technol.*, 2014.

[45]	"KiBox® To Go | Kistler." [Online]. Available: https://www.kistler.com/en/products/systems/kibox-to-go/.

[46]	Y. Ding, "Characterising combustion in diesel engines," Delft University of Technology, 2011.

[47]	D. Stapersma, *Diesel engines : A fundamental approach to performance analysis, turbocharging, combustion, emissions and heat transfer including thermodynamical principles. Vol. 3: Combustion*. Delft: TU Delft, 2009.

[48]	S. M. Krol, "Modelling and performance investigation of anode-off gas combustion in an IC engine for power generation," Delft Universty of Technology, 2018.

[49]	Y. Sun, H. Wang, C. Yang, and Y. Wang, "Development and validation of a marine sequential turbocharging diesel engine combustion model based on double Wiebe function and partial least squares method," *Energy Convers. Manag.*, vol. 151, pp. 481–495, Nov. 2017.

[50]	F. Maroteaux, C. Saad, and F. Aubertin, "Development and validation of double and single Wiebe function for multi-injection mode Diesel engine combustion modelling for hardware-in-the-loop applications," *Energy Convers. Manag.*, vol. 105, pp. 630–641, Nov. 2015.

[51]	H. Yasar, H. S. Soyhan, H. Walmsley, B. Head, and C. Sorusbay, "Double-Wiebe function: An approach for single-zone HCCI engine modeling," *Appl. Therm. Eng.*, vol. 28, no. 11–12, pp. 1284–1290, Aug. 2008.

[52]	F. Baldi, G. Theotokatos, and K. Andersson, "Development of a combined mean value-zero dimensional model and application for a large marine four-stroke Diesel engine simulation," *Appl. Energy*, vol. 154, pp. 402–415, 2015.

[53]	Y. Yeliana, C. Cooney, J. Worm, D. J. Michalek, and J. D. Naber, "Estimation of double-Wiebe function parameters using least square method for burn durations of ethanol-gasoline blends in spark ignition engine over variable compression ratios and EGR levels," *Appl. Therm. Eng.*, vol. 31, no. 14–15, pp. 2213–2220, Oct. 2011.

[54]	A. M. Shivapuji and S. Dasappa, "Experiments and zero D modeling studies using specific Wiebe coefficients for producer gas as fuel in spark-ignited engines.", *J. Mechanical Engineering Science*, 227(3) 504–519, 2012

[55]	H. Cho, S. R. Krishnan, R. Luck, and K. K. Srinivasan, "Comprehensive uncertainty analysis of a Wiebe function-based combustion model for pilot-ignited natural gas engines."

[56]	K. Ishii, T. Sasaki, Y. Urata, K. Yoshida, and T. Ohno, "Investigation of cyclic variation of IMEP Under lean burn operation in spark-ignition engine," *SAE Trasnsactions*, vol. 1, 1997.

[57]	G. a. Karim, I. Wierzba, and Y. Al-Alousi, "Methane-hydrogen mixtures as fuels," *Int. J. Hydrogen Energy*, vol. 21, no. 7, pp. 625–631, 1996.

[58]	I. Georgescu, D. Stapersma, L. M. Nerheim, and B. Mestemaker, "Characterisation of large gas and dual-fuel engines," *MTZ Ind.*, pp. 64–71, 2016.

[59]	F. Ma, Y. Wang, H. Liu, Y. Li, J. Wang, and S. Ding, "Effects of hydrogen addition on cycle-by-cycle variations in a lean burn natural gas spark-ignition engine," *Int. J. Hydrogen Energy*, vol. 33, no. 2, pp. 823–831, 2008.

[60]	J. Wang, H. Chen, B. Liu, and Z. Huang, "Study of cycle-by-cycle variations of a spark ignition engine fueled with natural gas-hydrogen blends," *Int. J. Hydrogen Energy*, vol. 33, no. 18, pp. 4876–4883, 2008.

[61]	F. Ma, S. Ding, Y. Wang, Y. Wang, J. Wang, and S. Zhao, "Study on combustion behaviors and cycle-by-cycle variations in a turbocharged lean burn natural gas S.I. engine with hydrogen enrichment," *Int. J. Hydrogen Energy*, vol. 33, no. 23, pp. 7245–7255, 2008.

[62]	Z. Huang, L. Liu, D. Jiang, Y. Ren, B. Liu, K. Zeng, and Q. Wang, "Study on cycle-by-cycle variations of combustion in a natural-gas direct-injection engine," *Proc. Inst. Mech. Eng. Part D J. Automob. Eng.*, vol. 222, no. 9, pp. 1657–1667, 2008.

[63] B. Huang, E. Hu, Z. Huang, J. Zheng, B. Liu, and D. Jiang, "Cycle-by-cycle variations in a spark ignition engine fueled with natural gas-hydrogen blends combined with EGR," *Int. J. Hydrogen Energy*, vol. 34, no. 19, pp. 8405–8414, 2009.

[64] H. Spliethoff, U. Greul, H. Maier, and K. R. G. Hein, "Low-Nox combustion for pulverized coal - A Comparison of Air Staging and Reburning," in *The Institute of Energy's Second International Conference on Combustion & Emissions Control*, 1995, pp. 61–70.

[65] G. J. Nebel and M. W. Jackson, "Some Factors Affecting the Concentration of Oxides of Nitrogen in Exhaust Gases from Spark Ignition Engines," *J. Air Pollut. Control Assoc.*, vol. 8, no. 3, pp. 213–219, 1958.

[66] D. Stapersma, *Diesel Engines: A fundamental approach to performance analysis, turbocharging, combustion, emissions and heat transfer including thermodynamical principles: Vol. 4: Emissions and heat transfer*, vol. 4, no. April. 2010.

[67] D. Stapersma, *Diesel engines : A fundamental approach to performance analysis, turbocharging, combustion, emissions and heat transfer including thermodynamical principles. Vol. 2: Turbocharging*. Delft, 2010.